PALEOCEANOGRAPHY, VOL. 23, PA3207, doi:10.1029/2008PA001610, 2008



# Ensemble, water isotope–enabled, coupled general circulation modeling insights into the 8.2 ka event

Allegra N. LeGrande[1] and Gavin A. Schmidt[1]

Received 13 February 2008; revised 14 April 2008; accepted 2 May 2008; published 19 July 2008.

[1] Freshwater forcing has long been postulated as a catalyst for abrupt climate change because of its potential to interfere with thermohaline circulation (THC). The most recent example may have occurred about 8.2 ka ago with the sudden drainage of glacial lakes Agassiz and Ojibway into the Hudson Bay. We perform an ensemble of simulations for this freshwater release using the fully coupled atmosphere ocean general circulation model, Goddard Institute for Space Studies ModelE-R. In all cases, simulated effects include reduced ocean heat transport and enhanced atmospheric heat transport in the Atlantic, increased surface albedo (through greater low cloud and sea ice cover), and local cooling of up to 3°C. Our suite of ensemble experiments allows us to examine the importance of the initial ocean state, in particular the presence or absence of Labrador Sea Water, in controlling the magnitude and length of the climate response. Water isotope tracers included in this model provide an improved means for direct comparisons of the modeled tracer response to water isotope–based, climate proxy data. Comparison of model simulations to data implies that there was an abrupt approximate halving of Atlantic THC, hence providing strong support for the hypothesis that the 8.2 ka event was caused by an abrupt release of fresh water into the North Atlantic.

**Citation:** LeGrande, A. N., and G. A. Schmidt (2008), Ensemble, water isotope–enabled, coupled general circulation modeling insights into the 8.2 ka event, *Paleoceanography*, *23*, PA3207, doi:10.1029/2008PA001610.

## 1. Introduction

[2] The 8.2 ka (8200 years B.P.) event was the most recent major abrupt cooling event in the Greenland ice core records [*Alley et al.*, 1997; *Thomas et al.*, 2007] and is postulated to have been triggered by the collapse of the Hudson Bay ice dome [*von Grafenstein et al.*, 1998]. The subsequent drainage of freshwater glacial Lakes Agassiz and Ojibway into the Hudson Bay [*Barber et al.*, 1999] could have interfered with the density-driven, thermohaline circulation (THC) in the North Atlantic (North Atlantic Deep Water (NADW)) by diminishing the density of upper ocean waters [*Broecker et al.*, 1985].

[3] The observational evidence for the abrupt event at 8.2 ka is most striking in the immediate vicinity of the North Atlantic basin. While there have been suggestions that evidence for an event at ~8.2 ka exists outside of this region [*Alley and Ágústsdóttir*, 2005], it is probable that this abrupt regional North Atlantic event is superimposed on and sometimes confused with a wider-spread, millennial-scale event [*Rohling and Pälike*, 2005]. The abrupt 8.2 ka event as defined in the Greenland ice cores likely lasted only ~160 years [*Thomas et al.*, 2007], with a peak cooling lasting 60–70 years. Thus far, convincing proxy records for such an abrupt event are confined to the North Atlantic and immediate surrounding regions [*Schmidt and Jansen*, 2006], notably including records of cooling temperatures in the east Norwegian Sea [*Risebrobakken et al.*, 2003], United Kingdom [*Marshall et al.*, 2007], southern Germany [*von Grafenstein et al.*, 1998], and a southward migration of the Atlantic Intertropical Convergence Zone (ITCZ) [*Haug et al.*, 2001]. We address only the short North Atlantic event, and limit our data comparisons likewise.

[4] There are several important questions that arise from these observations: Is the proxy climate evidence consistent with a freshwater event and slowdown of THC? Are there possible confounding factors to the interpretation of proxy records? The apparent lack of evidence for abrupt oceanic cooling in the northwestern North Atlantic has led to a speculation for another mechanism; e.g., the collapse of the remnant Hudson Bay ice dome (an orographic change) and disappearance of the glacial lakes may have significantly altered atmospheric circulation [*Hillaire-Marcel and de Vernal*, 1995].

[5] Previous work using Earth (system) models of intermediate complexity [*Bauer et al.*, 2004; *Renssen et al.*, 2001, 2002; *Wiersma and Renssen*, 2006] applied an approximately 8.2 ka event sized freshwater pulse to the North Atlantic of 1.5 to $5 \times 10^{14}$ m$^3$, larger than the *Clarke et al.* [2004] paleohydraulic modeling estimates of 0.79–$1.57 \times 10^{14}$ m$^3$, but within the range suggested by geologic evidence for the volume of Lake Agassiz at 8.4 ka (~$2 \times 10^{14}$ m$^3$ [*Barber et al.*, 1999] and $5 \times 10^{14}$ m$^3$ [*von Grafenstein et al.*, 1998]). The modeled responses of these studies to this approximately sized freshwater forcing for the 8.2 ka event were highly variable, though broadly consistent with the paleoclimate proxy records of past climate change. The more recent coupled GCM study by *LeGrande et al.* [2006] utilized several model tracers with

[1]Center for Climate Systems Research, NASA Goddard Institute for Space Studies, New York, New York, USA.


0883-8305/08/2008PA001610$12.00

**Table 1.** Isotopically Depleted Fresh Water Added to the Hudson Bay Surface in 12 Fully Coupled Simulations[a]

| Run | Initial NADW State | MWP Rate (Sv) | Length MWP (years) | MWP Volume ($m^3$) | Sea Level Rise (cm) | Maximum Decadal Δ NADW (%) | Anomaly Duration (years) |
|---|---|---|---|---|---|---|---|
| WK 5 Sv × 1 year | WK | 5.0 | 1.0 | $1.577 \times 10^{14}$ | 43 | −31.6 | 120 |
| WK 5 S v × 2 year | WK | 5.0 | 2.0 | $3.154 \times 10^{14}$ | 87 | −51.0 | 180 |
| WK 5 Sv × 0.5 year | WK | 5.0 | 0.5 | $0.788 \times 10^{14}$ | 22 | −28.5 | 100 |
| WK 2.5 Sv × 1 year | WK | 2.5 | 1.0 | $0.788 \times 10^{14}$ | 22 | −32.1 | 145 |
| ST10 5 Sv × 2 year | ST10 | 5.0 | 2.0 | $3.154 \times 10^{14}$ | 87 | −60.4 | 100 |
| ST10 5 Sv × 1 year | ST10 | 5.0 | 1.0 | $1.577 \times 10^{14}$ | 43 | −52.9 | 90 |
| ST 5 S v × 1 year | ST | 5.0 | 1.0 | $1.577 \times 10^{14}$ | 43 | −50.1 | 60 |
| ST 5 Sv × 0.5 year | ST | 5.0 | 0.5 | $0.788 \times 10^{14}$ | 22 | −37.5 | 40 |
| ST 5 Sv × 0.25 year | ST | 5.0 | 0.25 | $0.394 \times 10^{14}$ | 11 | −38.2 | 30 |
| ST 2.5 Sv × 1 year | ST | 2.5 | 1.0 | $0.788 \times 10^{14}$ | 22 | −53.6 | 45 |
| ST 2.5 Sv × 0.5 year | ST | 2.5 | 0.5 | $0.394 \times 10^{14}$ | 11 | −27.9 | 35 |
| ST 1.25 Sv × 1 year | ST | 1.25 | 1.0 | $0.394 \times 10^{14}$ | 11 | −25.4 | 40 |

[a]The simulations were started from two "base" states, different points in a long control run, characterized by relatively strong (ST) and weak (WK) overturning circulation. In the ST case, two runs were started 10 years later than other runs in this set (ST10). Anomaly duration is defined as the time it took the simulated NADW to return and stay above −5% of the control run. Sea level rise is approximated given the surface area of the modern ocean.

proxy record analogs to facilitate an ensemble of model to data comparisons and found a broad range of climate responses to a smaller range of freshwater forcing (0.79–$1.57 \times 10^{14} m^3$, consistent with the *Clarke et al.* [2004] estimates), with an ensemble mean halving of NADW formation closely resembling proxy records of the 8.2 ka event. Importantly, all studies suggested simulated responses to similar freshwater forcings are potentially nonlinear; i.e., sensitive to the exact starting conditions and not solely predictable from the size and rate of the initial freshwater forcing.

[6] Several questions arise from this previous modeling work: How sensitive is the climate response to the size and volume of forcing, and how dependent is it on the base climate? What mechanisms can explain the range of responses, and can this range provide the insight into proxy climate records?

[7] Here we use a fully coupled atmosphere-ocean general circulation model (GCM) that explicitly tracks water isotopes throughout the hydrologic cycle enabling us to examine not only whether this hypothetical freshwater forcing is consistent with the proxy evidence as in [*LeGrande et al.*, 2006], but also whether the relationships between proxies and climate are robust (e.g., following *Schmidt et al.* [2007]) during abrupt climate change events. We include 12 experiments in our analysis in order to diagnose the climate signal, related to the meltwater pulse (MWP) as well as the envelope of possible noise. We assess the important mechanisms of change through analyzing a suite of simulations (Table 1) that include (1) small perturbations of the initial conditions, "weather," and (2) two base states of the climate. One base state is more analogous to the modern world where NADW is produced in the northeastern through the northwestern (Labrador Sea) Atlantic. While the other is (fortunately) somewhat more analogous to conditions 8000 years ago where deep water production was dominated by that in the central to northeastern Atlantic [*Hillaire-Marcel et al.*, 2001]. The presence of deep water production in the northwestern Atlantic has been suggested as important in controlling modeled response to freshwater forcing. In intermediate complexity models freshwater corrections can be applied to approximate extra fresh water from the melting of the Laurentide Ice Sheet [*Wiersma et al.*, 2006]; these models imply the presence of this melting was important to controlling the size of the 8.2 ka event. The simulated range here was not induced; rather, it occurred through integration of a long control run; we capitalize on this useful, unforced range of initial conditions. It is in that sense an ensemble of opportunity.

## 2. Methods

### 2.1. Model Description

[8] GISS ModelE-R (Goddard Institute for Space Studies ModelE-R) is a fully coupled atmosphere/ocean GCM that was used for simulations in support of the Intergovernmental Panel on Climate Change 4th Assessment Report [*Randall et al.*, 2007]. The experiments here use the M20 version of ModelE whose horizontal resolution is 4° × 5°, with a 20 vertical layer atmosphere up to 0.1 hPa height [*Schmidt et al.*, 2006] coupled to the 13-layer Russell Ocean model of the same horizontal resolution [*Liu et al.*, 2003; *Russell et al.*, 1995, 2000]. This ocean model is non-Boussinesq, mass conserving, and has a full free surface. Fresh water is treated in a "natural" way; that is, the addition of fresh water increases the free surface and reduces salinity purely through dilution. No equivalent salt fluxes or flux adjustments are used allowing for the prognostic calculation of water isotope to salinity relationships. All boundary conditions and atmospheric composition are appropriate to the preindustrial period (circa 1880).

[9] Water tracers ($^1H_2^{16}O$, "normal" water; $^2H^1H\,^{16}O$, $\delta$D; $^1H_2^{18}O$, $\delta^{18}$O; where $\delta \equiv [(R_{std}/R_{smow}) - 1] \times 1000$) are included in the atmosphere, sea ice, and ocean and are tracked through all stages of the hydrologic cycle [*Schmidt et al.*, 2007]. These isotopes are advected like water through the model, but at each phase change, an appropriate fractionation is performed [*Schmidt et al.*, 2005], explicitly determining equilibrium fractionation and parameterizations accounting for kinetic fractionations.

[10] The control simulation was initialized from the 2001 World Ocean Atlas [*Conkright et al.*, 2002] and run for

1000 years, with no change in model forcing. During the initialization, a number of transient, quasi-stable states occurred before the model reached a more robust equilibrium. The associated small drift in the ocean is indicated by the temperature in the deepest ocean level increasing around 0.06°C per century. The model quasi-steady states have an expression in surface conditions in the ocean and atmosphere, and thus allow a limited exploration of the impact of the "base climate state" on the modeled response.

[11] We chose two base states that are distinct in their relative strength in NADW formation, defined here as the Atlantic overturning stream function at 48°N and 900 m depth. The decades after year 200 of the control, (hereinafter referred to as the weak initial NADW case (WK)) are characterized by a weak, variable overturning (NADW: 12 ± 1.7 Sv) (1 Sv $\equiv 1 \times 10^6$ m$^3$/s). While the decades after year 600 of the control, (hereinafter referred to as the strong initial NADW case (ST)) are characterized by a strong, relatively stable overturning circulation (NADW: 22 ± 1.2 Sv), closer to the ultimate equilibrium.

[12] The maximum overturning circulation in the Atlantic is slightly larger, highly correlated (r > 0.65) to this NADW formation index, but more variable. The maximum overturning circulation in the WK simulations is 20.8 ± 2.2 Sv, while it is 32.9 ± 2.3 Sv for the ST simulations. Potential density at the surface of the deep water formation areas is 27.2–27.3 kg/m$^3$, though the temperature and salinity characteristics of these two periods are different. The ST control is associated with relatively warmer, more saline NADW (T: ~5.3°C, S: ~35.1 psu, $\delta^{18}O_{seawater}$: ~0.14‰) compared to the WK control (T: ~3.1°C, S: ~34.9 psu, $\delta^{18}O_{seawater}$: ~0.07‰); observed NADW is 2°C–4°C, 34.9 psu [*Open University Course Team*, 2001], and 0.2‰ (at the core of NADW [*LeGrande and Schmidt*, 2006]).

[13] Since the location of the maximum overturning circulation can change in response to the MWP forcing, it is a less robust indicator of climate change. Alterations in NADW formation (at 48°N, 900 m) strength in these simulations are highly correlated with alterations in the maximum overturning circulation in the Atlantic and are a more robust indicator of climate change in the North Atlantic.

### 2.2. Experiment Design

[14] Results are from a suite of 12 model experiments with MWP forcing ranging from as large as 10 Sv years (1 Sverdrup year ≈ $0.315 \times 10^{14}$ m$^3$ ≈ 9 cm sea level) to as small as 1.25 Sv years applied at rates between 1.25 and 5 Sv (Table 1). *LeGrande et al.* [2006] analyzed an ensemble of a subset of these simulations, specifically the 2.5 to 5 Sv year pulses that bracket best guess estimates from paleohydraulic and geologic studies of the 8.2 ka event [*Barber et al.*, 1999; *Clarke et al.*, 2004; *Teller et al.*, 2002; *von Grafenstein et al.*, 1998].

[15] Meltwater (T: 0°C; S: 0 psu; $\delta^{18}$O: −30‰) is spread equally over the Hudson Bay grid boxes at a prescribed rate and duration (see Table 1); this $\delta^{18}$O is at the lower end of estimates for the isotopic composition of Lake Agassiz prior to final drainage (C. Hillaire-Marcel, personal communication, 2007). We add a MWP tracer that is initialized to 0 everywhere, except for the MWP itself which is specified at 1; the subsequent concentration of this tracer allows us to explicitly remove or scale the $\delta^{18}$O of the MWP during the remainder of the simulation. This fresh water represents additional water added to the climate system and raises global sea level by ~12 to 90 cm.

[16] Four simulations are started from the WK case (control year 200), and these simulations have a slow recovery time, requiring up to 180 years of model simulation. (Recovery here is defined as NADW formation returning to and remaining above 95% of the control run mean NADW formation.) In the remaining eight simulations, the initial conditions were taken from the ST case (control year 600); two of these were started 10 years later than the others (i.e., control year 610, hereinafter referred to as ST10) to provide a more complete suite of ensemble members. The faster recovery time in the ST (and ST10) simulations required up to 100 years of model simulation for NADW recovery (Table 1).The WK case exhibits decadal variability which has higher amplitude than the ST case; thus, as given by *LeGrande et al.* [2006], we reduce the influence of this unforced variability through examining "decadal" results: the 10-year mean of the MWP experiment less the 30-year mean of the relevant control years. Hereinafter, for simplicity, NADW formation strength at 48°N, 900m is used as a simple metric (index) against which other model comparisons can be made. This analysis effectively reduces the problem to one dimension, allowing the diagnosis of NADW-correlated climate change, consistent climate changes related to the MWP, and the noise beyond the two.

## 3. Results

[17] All simulations show a significant decrease in NADW formation. Within each simulation, however, the exact timing, magnitude, and length of the NADW perturbation, as well as the associated global climate responses, are highly variable and not simply predictable from the initial forcing alone (Figure 1), consistent with previous studies that labeled this type of response as "stochastic" [*Bauer et al.*, 2004; *Renssen et al.*, 2001].

[18] After the meltwater injection, sea surface density decreases dramatically across the surface northern North Atlantic as the fresh water spreads across the area. Initial surface density ($\rho$) varies by less than 0.1 kg/m$^3$ in all simulations, and $\rho$ anomalies range from about 5 kg/m$^3$ for 10 Sv year pulses to as little as approximately 1 kg/m$^3$ for 1.25 Sv year pulses (Figure 1a). These immediate (within 2–3 years) large anomalies in northern North Atlantic $\rho$ precede the maximum decreases in NADW formation, and completely dissipate within the first decade of the simulations (Figures 1b and 1d). This phasing illustrates that anomalies in NADW formation are associated with the alterations in the ocean's density structure, not the absolute value of surface density change. Further, simulations with very similar forcing can and do yield different climate responses. Here we explore the climate mechanisms in ModelE-R that give rise to the range of climate responses.

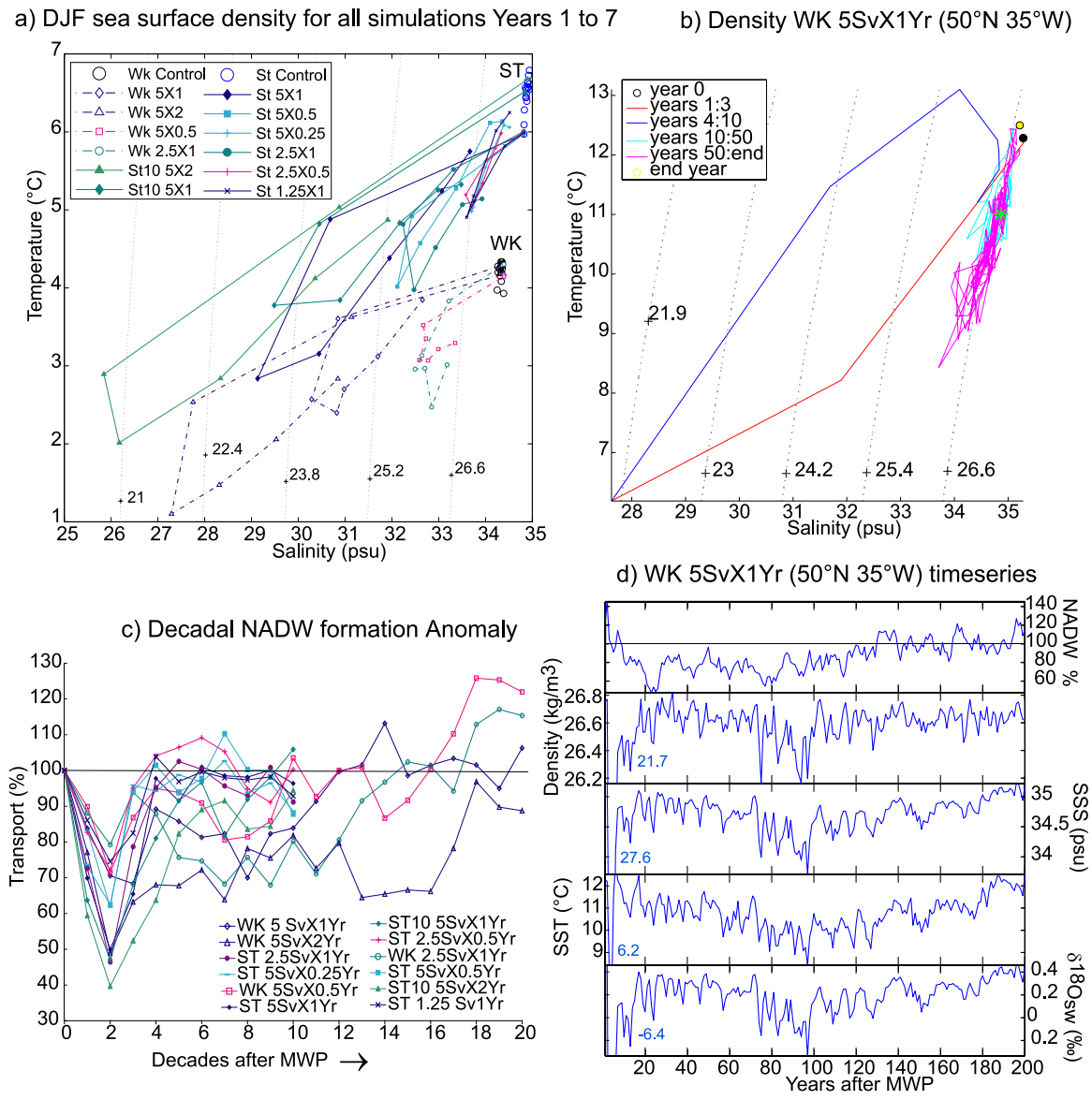


**Figure 1.** (a) Sea surface temperature versus salinity in the North Atlantic (50°N–70°N) for all simulations during the first seven winters (December, January, and February (DJF)) after the initial MWP. (b) Annually averaged sea surface conditions for the WK 5 Sv × 1 year case for a typical middle North Atlantic grid box (50°N, 35°W) for all years. (c) Percent transport anomaly in NADW formation for each 10-year average MWP simulation compared to the corresponding 30-year average control simulation. WK simulations have open symbols, ST simulations have solid symbols, and shapes correspond to rate and volume of forcing in Figures 1a and 1c. Isopycnals of potential density (kg/m$^3$: $\rho^* = \rho - 1000$) are in dashed gray lines in Figures 1a and 1b. (d) For the WK 5 Sv × 1 year simulation, annual percent anomaly in NADW formation, sea surface $\rho^*$ (kg/m$^3$), sea surface salinity (SSS) (psu), SST (°C), and surface $\delta^{18}O_{seawater}$ (‰). The minimum (from year 4) is noted in blue.

[19] There are three possible sources of variability within this suite of simulations that we address (1) interannual ocean variability (e.g., ST 5 Sv × 1 year versus ST10 5 Sv × 1 year), (2) small changes in the forcing (e.g., WK 2.5 Sv × 1 year versus WK 5 Sv × 0.5 year and ST 2.5 Sv × 1 year versus ST 5 Sv × 0.5 year), and (3) variability of base state (i.e., WK case versus ST case simulations) given identical forcing.

### 3.1. Sources of Variability

[20] The ST and ST10 simulations have the same base state, but slightly different initial conditions; they were started 10 model years apart; they differ from one another only in the exact "weather" conditions in the model (through interannual ocean variability). The shape of the NADW anomaly in these two is highly similar, and the maximum NADW change is statistically equivalent

(Figure 1c). The small differences between these simulations do not arise until the end of NADW recovery. The ST initial condition is characterized by a smoother, always positive recovery, compared to a slightly more variable recovery in the ST10 initial condition. The magnitudes of climate anomalies during reduced NADW are highly similar between the two, indicating that in this GCM for this pair of "weather" conditions, interannual ocean variability did not have a large impact on the modeled response.

[21] The pairs of simulations with identical base states and initial conditions, but slightly different forcings (varying the rate, not total volume of MWP: the WK 5 × 0.5/WK 2.5 Sv × 1 year pair, the ST 5 Sv × 0.5 year/ST 2.5 Sv × 1 year pair, and the three 1.25 Sv year simulations) show comparable reductions in NADW formation, though a larger range than that of the paired initial conditions (Figure 1c). Within each pair, the simulation with the higher input rate, delivers a greater amount of fresh water in a shorter amount of time and that yields greater sea surface height anomalies in the Hudson Bay. This sea surface height anomaly causes a greater pressure gradient in the surface ocean that flushes the fresh water out through the Hudson Strait more rapidly, reinforcing the faster delivery of fresh water into the open ocean. Climate differences from these pairs are subsequently short-lived and largely localized to the area around the meltwater. All of these pairs have similar responses in magnitude and length of anomaly and climate response, except for the decadal NADW response of the ST 2.5 Sv × 1 year/ST 5 Sv × 0.5 year pair which warrants further discussion.

[22] Local anomalies between the ST 2.5 Sv × 1 year/ST 5 Sv × 0.5 year pair arise in the first decade before the distinctive physical properties of the MWP have dissipated. The modeled NADW response while reducing is highly similar at annual time scales. However, in the years 9–16, the simulation with the slower delivery maintains near (within 1$\sigma$) maximum NADW perturbation, while the faster rate reaches maximum NADW change for only a year and recovers. This contrast is likely due to small differences between the "weather" (stochastic response) in the two simulations, perhaps initiated by the difference in timing when the fresh water arrives into the open Atlantic. The discrepancy indicated by the decadal average NADW formation change is a result of these small annual differences that induce small magnitude NADW formation changes, yielding an apparently larger NADW and climate perturbation in the simulation with the lower rate.

[23] The final pair is between runs with identical forcing, but different base states; i.e., ST/WK 5 Sv × 1 year, ST/WK 5 Sv × 0.5 year, ST/WK 2.5 Sv × 1 year, and ST/WK 5 Sv × 2 year. The base case does give rise to significant differences in the magnitude, length, and structure of the modeled response (Figure 1c). Responses in the WK simulations typically have half the magnitude of NADW formation (and climate) anomalies, but persist for 2 to 3 times as long as those in the ST simulations.

[24] To examine why the differences are so profound, we examine the differences between the base case cases. The ST case has enhanced overturning circulation relative to the WK case (22 Sv compared to 12 Sv), and deep convection in the southernmost Labrador Sea. The lack of Labrador Sea deep water formation in the WK case is coincidentally consistent with proxy inferences for deep water production from the early Holocene [*Hillaire-Marcel et al.*, 2001]. Additional overturning occurs in the ST case because it has saltier (and warmer) conditions in the NW Atlantic at the southern end of the Labrador Sea (Figure 2). Consistent with the deep convection in the NW Atlantic, the ST case is warmer and has a more negative freshwater balance (precipitation less evaporation plus river runoff) near the Labrador Sea which is thus relatively saltier, with enriched $\delta^{18}O_{seawater}$. The enhanced overturning in the ST case results in greater surface air temperature (SAT), higher sea surface temperature (SST), and heavier $\delta^{18}O_{precip}$ in the North Atlantic region in general (∼+1.3°C, ∼+0.37‰, Figure 2).

[25] The weaker overturning of the WK case requires a more stratified ocean with greater deep ocean salinities than in the ST case; surface salinities of the ST case are globally ∼ +0.32 psu greater. The stratification in the WK case means that the vertical density gradients are larger in the beginning, and the surface MWP enhances this gradient. Given these differences, the ST case has the larger MWP response not only because there is more overturning with which to interfere, but also, the ocean is less stratified, allowing a quicker dilution (through vertical mixing) of the MWP. Thus, the different magnitude of responses is likely a direct result of the different base climate conditions in the Atlantic.

[26] In the ST case, precipitation less evaporation plus river runoff is lower particularly in the northern tropics and at deep water formation latitudes. The ST case simulations are more sensitive to freshening, but more efficient at restoring salty sea surface conditions, leading to a larger anomaly, but quicker restoration of NADW formation. In addition, the WK case appears to have additional cooling initiated, not correlated with reduced NADW (Figure 3) yielding elongated climate anomalies.

### 3.2. Feedback Mechanisms

[27] SST changes in response to diminished overturning circulation and model feedbacks (e.g., albedo changes, clouds, sea ice, etc.); only a minor component of SST change is due to the heat content anomaly of the MWP itself. The distinctive physical properties of the MWP largely dissipate by the end of the first decade (Figure 1a).

[28] SST changes are highly correlated with NADW formation changes, and NADW formation changes can be used as a proxy for the pattern of SST and related climate changes associated with altered NADW [*LeGrande et al.*, 2006]. We apply a similar regression and scaling process used by *LeGrande et al.* [2006] (NADW percent formation changes versus climate (SAT, precipitation, etc.) scaled for the average percent NADW anomaly; the mixed case has −40% NADW [*LeGrande et al.*, 2006]; ST case has −51% NADW; and the WK case has −32% NADW). We determine ensemble mean response for both ST case simulations, WK case simulations, and mixed case [*LeGrande et al.*, 2006] allowing us to clearly distinguish the NADW response of each (Figure 3). The original mixed ensemble consists of 5 runs: ST 5 × 1, ST 5 × 0.5, ST 2.5 × 1, WK

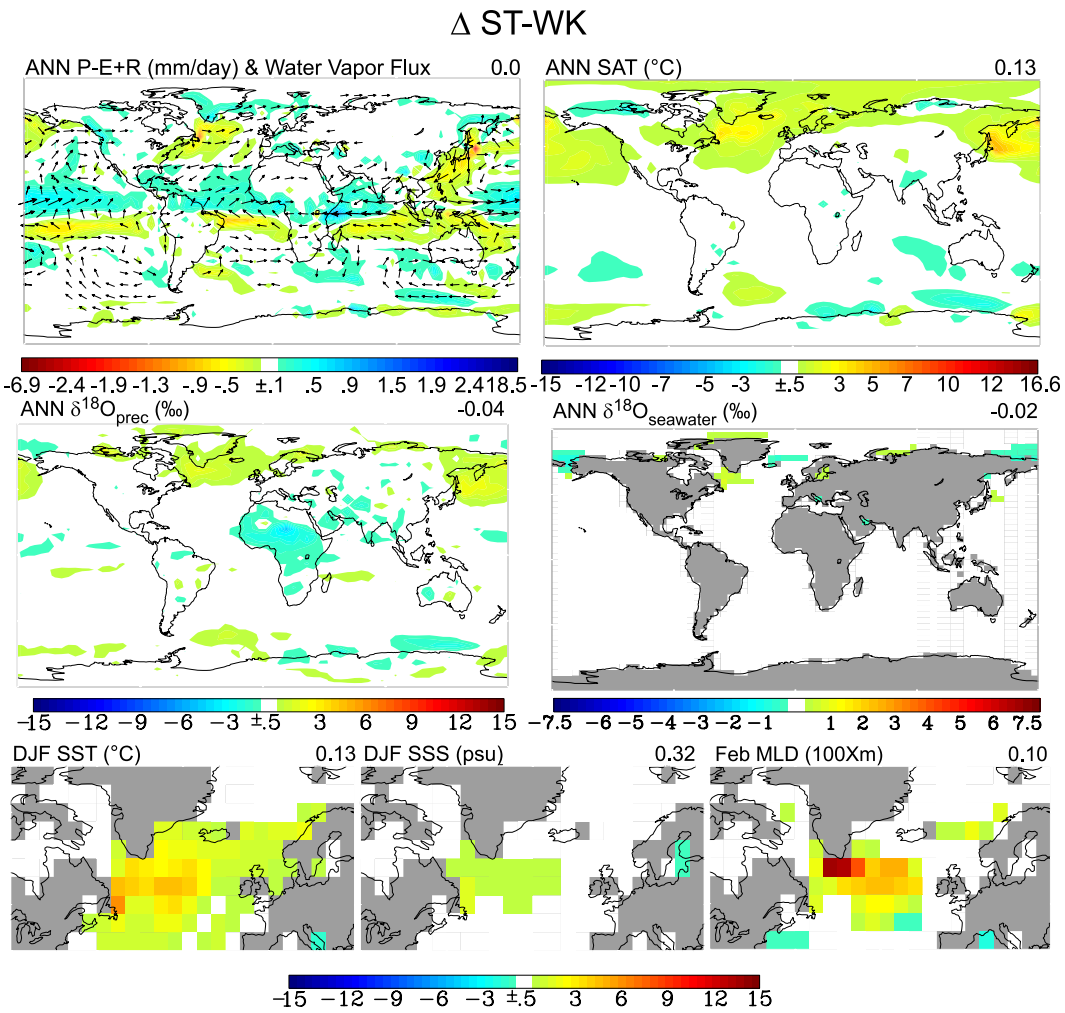


**Figure 2.** ST case less WK case with global means for each field appearing to the right of the heading for differences in (top) surface freshwater balance with water vapor flux overlain (direction) and surface air temperature, (middle) water isotope distribution in precipitation and surface waters, and (bottom) northern North Atlantic winter sea surface temperatures, winter salinities, and February mixed layer depths.

5 × 1, and WK 5 × 0.5. These particular members were chosen since the *Clarke et al.* [2004] estimates found the 5 Sv × 1 year and 5 Sv × 0.5 year forcing to produce the best match to observations; three ST cases were used compared to two WK cases to give both cases equal weight in the regression.

[29] The pattern of SAT changes associated with reduced NADW is highly similar in all three ensembles (Figure 3), consistent with patterns of SAT cooling from other models with North Atlantic freshwater forcing [*Stouffer et al.*, 2006]. This NADW-SAT pattern includes a strong North Atlantic cooling, particularly over surface areas of NADW production, with cooling that extends regionally into the Arctic, Europe, North America, somewhat into Asia, over the North Pacific. The NADW-related climate changes exhibit asymmetric responses in the Northern and Southern hemispheres, an expression of the bipolar seesaw [*Broecker*, 1998], similar to previous studies using older versions of the GISS model [*Rind et al.*, 2001].

[30] The individual ST simulations, during decade 2, when the maximum NADW anomalies occur, also closely resemble the pattern of temperature change from the regressions. However, the individual WK simulations have substantially more cooling in the Southern Hemisphere, and thus greater global cooling, differing from the WK case ensemble NADW regression pattern. The more complicated SAT anomaly structure of the WK case includes additional cooling across the Southern Hemisphere, indicating the importance of additional climate mechanisms. The southern hemisphere cooling pattern, in particular, is not captured in the WK NADW-SAT regression because southern hemisphere cooling and warming evolve on a different time scale than NADW slowdowns, cooling during the primary slowdown and between and during secondary and tertiary slowdowns of NADW.

[31] Because of the diminished NADW formation, all simulations have reduced northward ocean heat transport

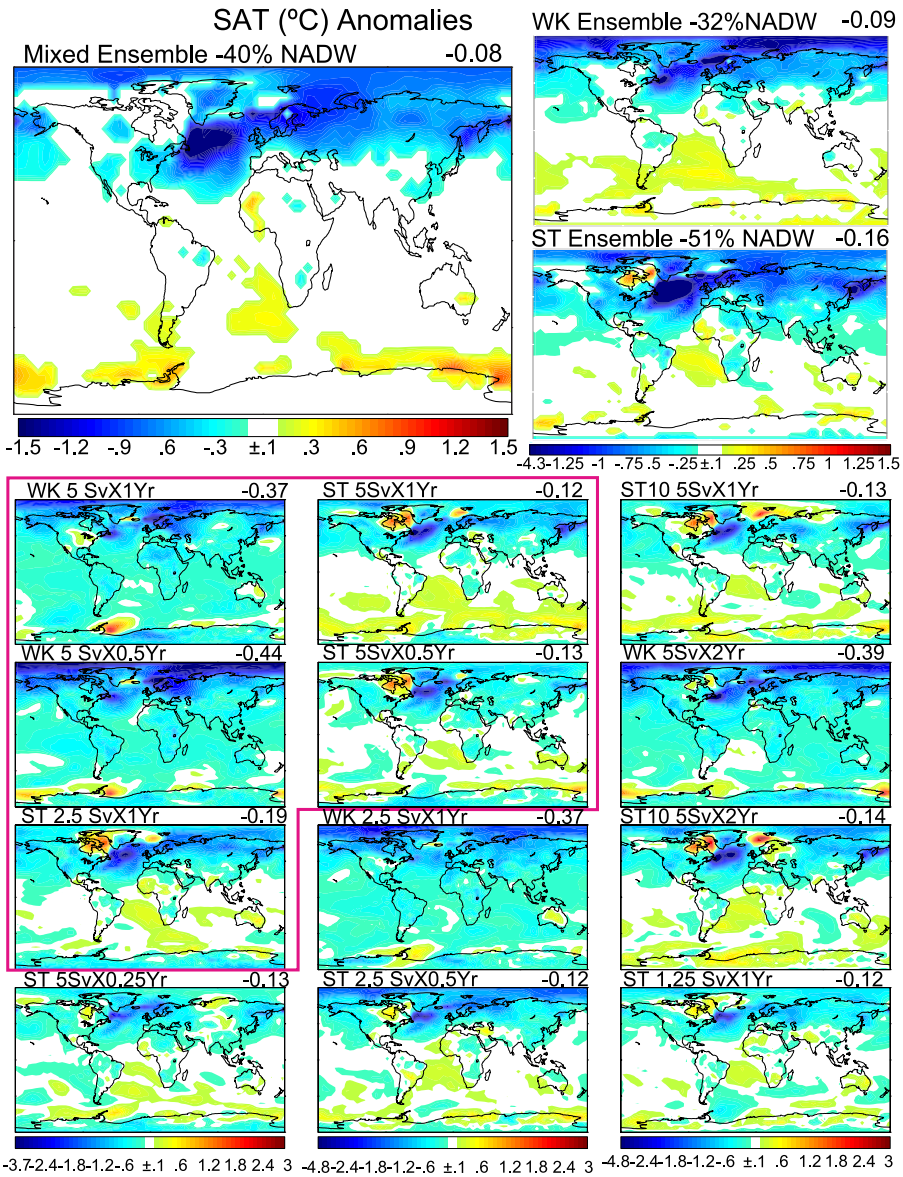


**Figure 3.** (top, left) Scaled −40% NADW formation ensemble mean SAT (°C) anomaly simulation (ensemble members outlined in pink) regression from *LeGrande et al.* [2006]. (top, right) Scaled −51% ST and −32% WK case ensemble mean anomalies. (bottom) Decade 2 SAT (°C) anomalies in each. Global mean anomalies are in the top right corner of each. Ensemble regressions show only changes where the slope is greater than $2\sigma_{slope}$.

(OHT). The mixed ensemble mean (40% NADW reduction) OHT anomaly is around −0.3 PW (petawatt ≡ $10^{15}$ watts) in the northern midlatitudes (∼30°–45°N). All simulations show that the largest OHT decreases occur in the midlatitudes of the Northern Hemisphere (Figure 4), particularly in the Atlantic region, where SST decreases are also greatest. The ST and WK case have different ensemble mean responses in heat transport. The markedly larger reduction in NADW formation in the ST cases leads to larger reductions in OHT. The two simulations with the largest anomalies are from the ST case: the 5 Sv × 2 year simulation (∼−0.5 PW), followed closely by the 2.5 Sv × 1 year simulation.

[32] The reduction in northward OHT is dominated by Atlantic changes, though some reductions also occur in the Pacific Ocean. Atlantic northward OHT becomes progressively reduced northward through the North Atlantic. This progression is greater in the ST case than the WK case. This dynamic is consistent with the more vigorous Atlantic Ocean circulation of the ST case.

[33] The atmosphere responds strongly to changes in the surface ocean. Northward atmospheric heat transport (AHT) increases by a maximum of 0.1–0.2 PW (across the mixed, ST, and WK case ensembles) providing a negative feedback and compensating in part for the diminished northward OHT, similar to other model results [*Zhang and Delworth*,

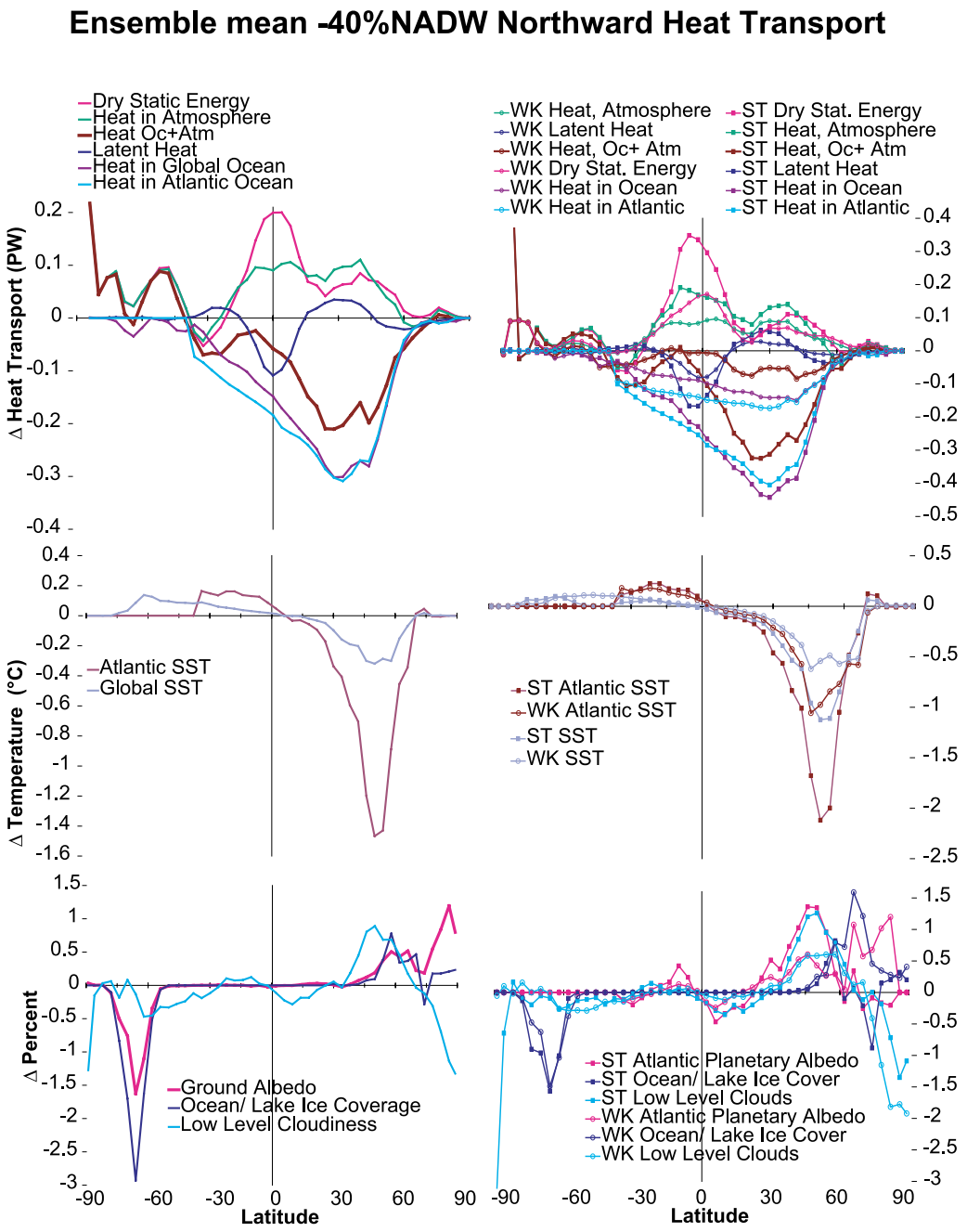


**Figure 4.** Ensemble mean (−40% NADW) zonal average anomalies in (top) northward heat transport and feedbacks: (middle) SST changes and (bottom) albedo-related changes. The WK case (−32% NADW) and ST case (−51% NADW) ensemble mean zonal average anomalies are shown on the right.

2005]. However, since AHT changes are of a smaller magnitude than the northward OHT reductions, total northward heat transport for the subtropics to midlatitudes still diminishes by between 0.18 and 0.35 PW; total northward heat transport decreases by around 0.2 PW in the mixed ensemble mean (Figure 4).

[34] AHT can be subdivided into two major categories: northward transport of dry static energy, and northward transport of latent heat. In the tropics, the Intertropical Convergence Zone (ITCZ) migrates southward and causes anomalies in these two components of opposite sign about the equator: dry static energy increases by around 0.2 PW, while latent heat decreases by around 0.1 PW. In the subtropics, both AHT components are positive in sign; but in midlatitudes, latent heat transport is decreased by a small amount because of a southward shift in precipitation. At high latitudes (>76°N), the changes in both are small.

[35] After the larger reduced northward OHT in the ST case, a faster, greater increase of northward AHT (compared to the WK case) contributes to the faster recovery time than

in the WK cases (Figure 5). The two responses differ in northward heat transport at around 35°S, or roughly the latitude of the southern tip of Africa, highlighting a contrast of greater Indian Ocean heat (~0.05 PW) and salt transport into the Atlantic Ocean in the ST case. OHT becomes proportionally much greater in the ST case in the Northern Hemisphere, with a 0.35 PW greater northward OHT at the latitude of the additional LSW convection. The ST case reduction in northward OHT does reduce this interbasin transport, but is dominated by reductions in OHT in the northern hemisphere (where OHT is relatively enhanced in the ST case compared to the WK case); enhanced ST case northward AHT also is dominated by changes in the equatorial to Northern Hemisphere.

[36] In the recovery from the MWP, positive salinity anomalies in the ST case start in the midlatitudes of the North Atlantic and propagate southward. This salinity anomaly begins forming immediately once the MWP water has dissipated, and it also contributes to the quicker restoration of NADW formation. In the WK case, the salinity recovers throughout the mid to North Atlantic roughly synchronous with the recovery of NADW formation. The salinity anomalies do not appear to lead the recovery in NADW formation in either case.

[37] There are at least two hypotheses for NADW formation recovery that require the restoration of salinity in the North Atlantic through advection to the northern North Atlantic from the south [*Broecker and Denton*, 1990]. In the first, enhanced advection of salty, warm Indian Ocean waters propagate northward and cause the recovery. In the second, the southward migration of the ITCZ allows salty surface waters to build up in the tropical Atlantic [*Broecker and Denton*, 1990]. The difference between the two base cases indicates that although the Indian Ocean interbasin transport is crucial in causing a difference in response between the base cases, it is not the source of salinity restoration in the Atlantic (and NADW reinitiation) (Figure 5). Likewise, salinity restoration in the North Atlantic does not begin in the tropics in either simulated case, indicating that the southward ITCZ migration and the related, though small, tropical salinity changes do not reinitiate the salinity restoration and restart NADW formation.

[38] The alterations in heat transport lead to feedbacks (in particular, sea ice and cloud cover alter albedo) that transmit the initial freshwater forcing from the surface North Atlantic to elsewhere into the climate system. In response to the diminished heat transport and alteration in SST structure, albedo across the northern North Atlantic increases (Figure 4). Decreased sea ice melting (or enhanced formation) as well as enhanced low cloud cover provides negative (cooling) feedbacks on the regional climate of the northern North Atlantic, providing an enhancing mechanism (to cooler SAT and advection) through which the ocean heat transport changes are transmitted to the surrounding land.

[39] The ST ensemble has the largest albedo changes centered around 45°N; the WK ensemble exhibits positive albedo changes at similar latitudes, but its largest albedo change is farther north, centered around 70°N. The cause of the more northern albedo change maximum is a consistent increase in ocean and lake ice across the WK simulations; these ice changes are not present in every ST simulation. In the Southern Hemisphere, both cases exhibit similar negative changes in ice cover, though the WK has an enhanced cloud cover feedback that persists and is not captured in the regression. In addition the WK anomalies have reduced net solar greater radiation (top of the atmosphere) of $-20-30$ W/m$^2$, though this causes the planetary albedo of the Southern Hemisphere to change very little. Tropical changes in both cases are similar and related to the southward migration of the ITCZ.

### 3.3. Comparisons to Paleoclimate Proxies

[40] The $\delta^{18}$O tracers in the model provide an opportunity to explore the impact of freshwater forcing on the proxy $\delta^{18}$O records of past climate change.

#### 3.3.1. Direct Meltwater Pulse Contribution to Proxy Changes

[41] We use a tracer of the MWP to track the relative contributions of the MWP itself and separate its "indirect" impact through climate-related $\delta^{18}$O changes (Figure 6). The majority of the distinctive, depleted meltwater $\delta^{18}$O is evaporated and then rains out in the first decade. It causes large $\delta^{18}O_{precip}$ anomalies of comparable magnitude to the climate component during the first decade after the initial MWP, particularly immediately over its source area (Hudson Bay), and eastward into the central northern North Atlantic. From decade 2 onward, the climate component of $\delta^{18}O_{precip}$ (Total-$\delta^{18}O_{precip}$ less MWP-$\delta^{18}O_{precip}$) is dominant everywhere. The early depleted MWP feature illustrates that a depleted $\delta^{18}O_{precip}$ signal not related to decreased temperature is possible in $\delta^{18}O_{precip}$ records whose precipitation sources (largely) include areas near the MWP release (i.e., the North Atlantic). However, since this feature is very short-lived, only very high resolution records such as ice cores or speleothems would likely display such a feature.

[42] In contrast, the MWP plays a larger role in influencing the oxygen isotopic composition of seawater ($\delta^{18}O_{seawater}$) than precipitation (Figure 6). The depleted $\delta^{18}$O of meltwater enhances the negative $\delta^{18}O_{seawater}$ anomalies in the northern North Atlantic because of climate changes, but dampens positive $\delta^{18}O_{seawater}$ anomalies in the GIN (Greenland Iceland Norwegian) seas and Arctic Ocean. Enriched $\delta^{18}O_{seawater}$ areas occur because (1) cooler SATs result in diminished precipitation over the catchment basins of Arctic Ocean and GIN Seas rivers, thus decreasing fresh, light $\delta^{18}$O river outflow and (2) diminished sea ice melting (increased ice formation only weakly, positively fractionates $\delta^{18}$O [*Craig and Gordon*, 1965; *Pfirman et al.*, 2004]), though ice changes are not present in every simulation.

#### 3.3.2. Surface Air Temperature ($\delta^{18}O_{precip}$)

[43] SAT is positively correlated with $\delta^{18}O_{precip}$ at middle to high latitudes (Figure 7). North America, South America, Europe, Greenland, and the North Atlantic region all show depleted $\delta^{18}O_{precip}$ anomalies.

[44] All ensemble mean results emphasize the decrease in $\delta^{18}O_{precip}$ across the North Atlantic basin, and surrounding regions. Western Greenland $\delta^{18}O_{precip}$ is particularly light, with further depletion eastward, and compares well to the

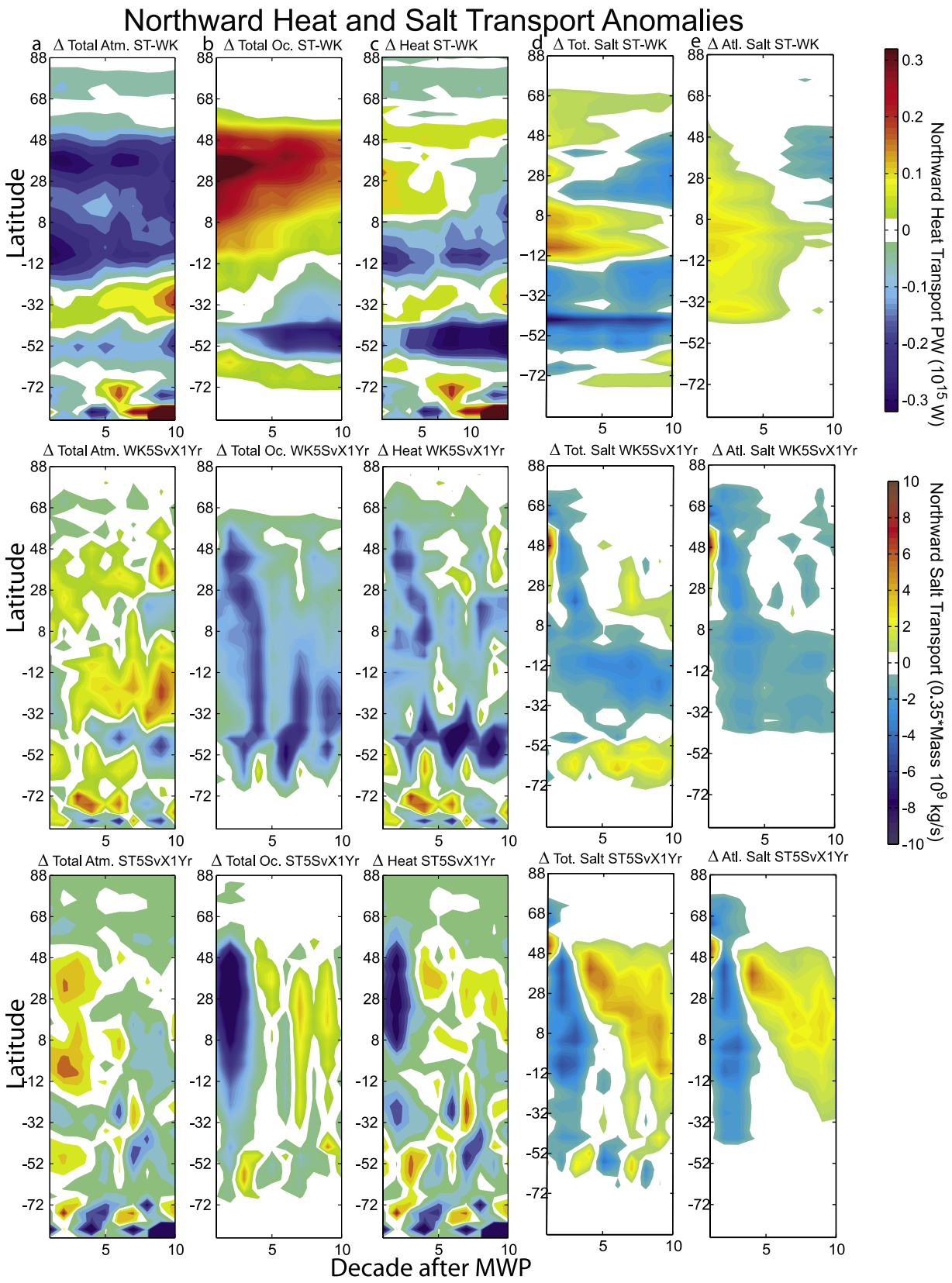


**Figure 5.** Anomalies in northward heat (PW) and salt (0.035 × mass $10^9$ kg/s) transport for (top) ST-WK case, (middle) WK 5 Sv × 1 year, and (bottom) ST 5 Sv × 1 year. (a) Total atmospheric heat transport (latent heat and dry static energy), (b) ocean heat transport, (c) total heat transport, (d) global salt transport, and (e) Atlantic salt transport.

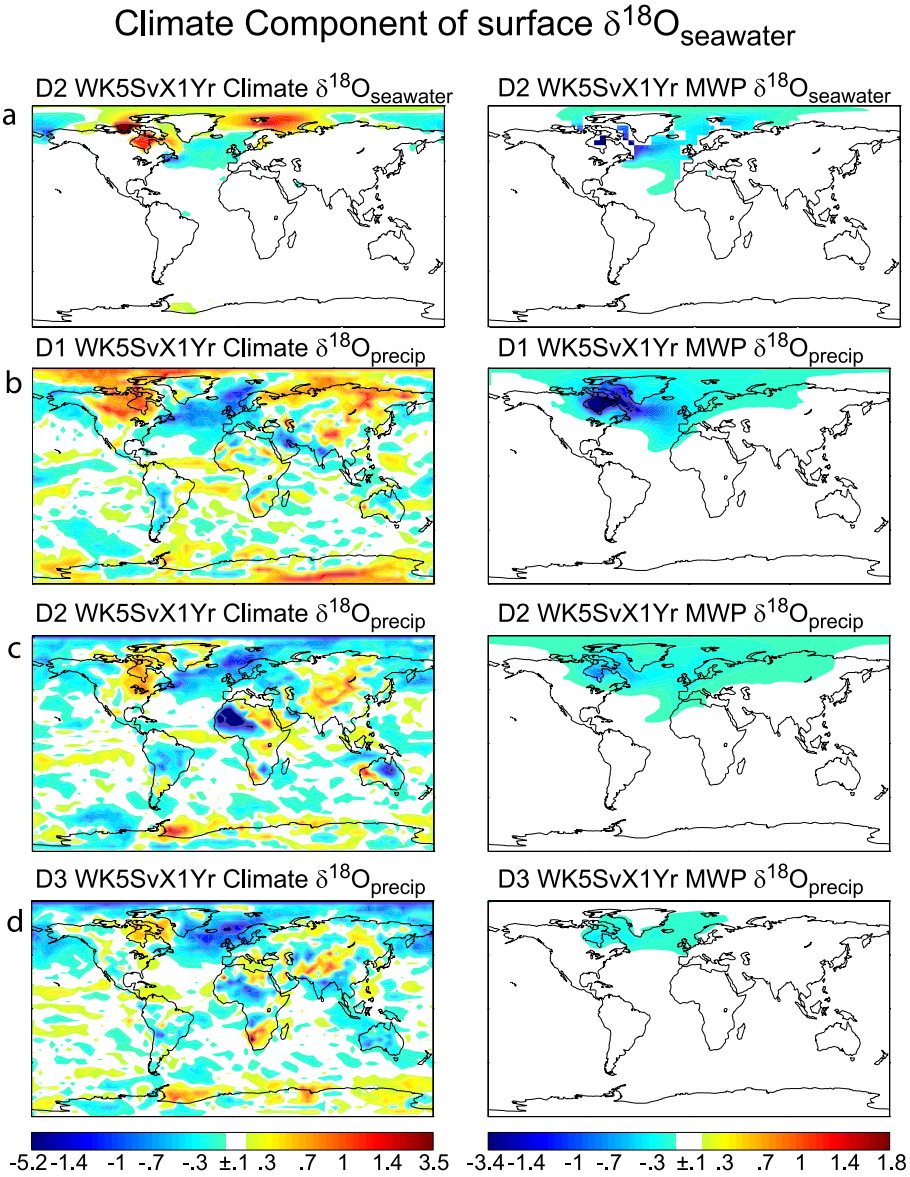


**Figure 6.** For WK 5 Sv × 1 year, (a) during decade 2, the climate component of (left) surface $\delta^{18}O_{seawater}$ anomalies (‰) is comparative to the (right) depleted MWP contribution (‰) in creating the surface $\delta^{18}O_{seawater}$ signal (‰). During decades (b) 1, (c) 2, and (d) 3 the (left) climate component of $\delta^{18}O_{precip}$ anomalies (‰) is less (decade 1) and then quickly exceeds (decades 2 and 3) the (right) depleted MWP contribution (‰).

observed −2‰ [*Thomas et al.*, 2007]. Enrichments in $\delta^{18}O_{precip}$ occur in some areas of Antarctica, but these results are not consistent across the simulations. Antarctic ice cores have been suggested as recording the 8.2 ka event [*Morrill and Jacobsen*, 2005]; however, anomalies at this time cannot be confirmed largely because of the temporal resolution required [*Masson et al.*, 2000]. Bands of relatively enriched (northern) and depleted $\delta^{18}O_{precip}$ in the tropics occur as a result of the southward ITCZ migration.

[45] West Africa shows a mixture of enriched and depleted $\delta^{18}O_{precip}$ values. However, this result is tenuous as a result of the small amount of precipitation in this region; small amounts of rainfall cause very noisy $\delta^{18}O_{pre\text{-}precip}$ fields and reduce the significance of signals in dry regions. Northeastern Africa though the Middle East, India, and northeast into Siberia show $\delta^{18}O_{precip}$ enrichments in the many of simulations, and the occurrences of this feature in WK and ST cases of larger and smaller volume MWPs and WK, ST, and mixed ensembles indicate that this feature is very robust.

[46] Interestingly, in the ensemble mean results for south and southeast Asia: despite small mixed positive and negative sign precipitation anomalies, $\delta^{18}O_{precip}$ still becomes enriched, particularly over south Asia, the Thailand peninsula, and into the Middle East (see Figure 7).

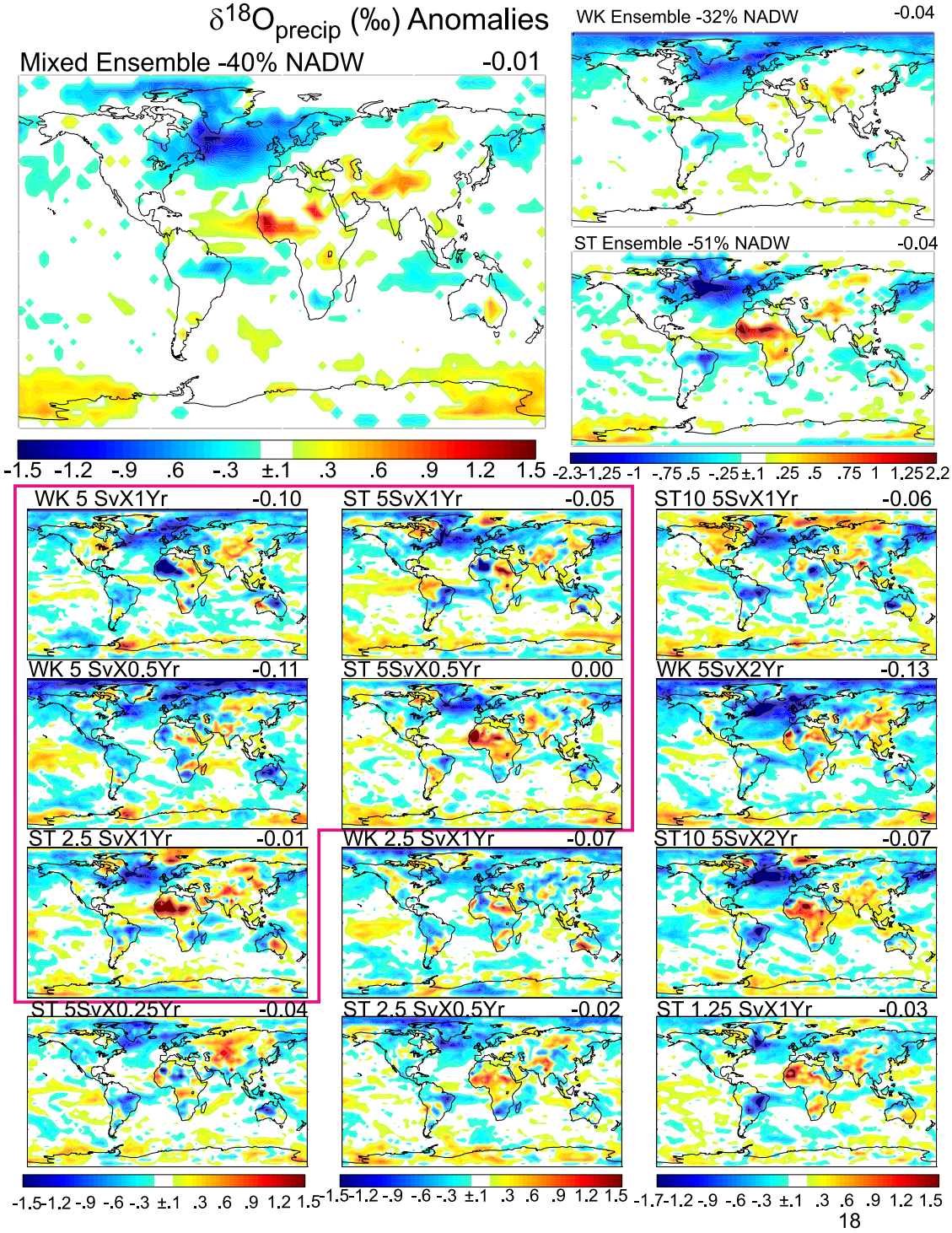


**Figure 7.** (top, left) Scaled −40% NADW formation ensemble mean $\delta^{18}O_{precip}$ (‰) anomaly (ensemble members outlined in pink) regression from *LeGrande et al.* [2006]. (top, right) Scaled −51% ST and −32% WK case ensemble mean anomalies. (bottom) The $\delta^{18}O_{precip}$ (‰) anomalies in each individual simulation during the second decade after the initial MWP. Mean anomalies are in the top right corner of each map. Ensemble regressions show only changes where the slope is greater than $2\sigma_{slope}$.

Changes in the North Atlantic and tropical $\delta^{18}O_{precip}$ could be anticipated from the precipitation and temperature anomalies. The south to central Asia changes in $\delta^{18}O_{precip}$ would not be anticipated based on changes in precipitation and SAT, and these anomalies are probably related to large-scale changes in the tropical hydrologic cycle (and alteration in the $\delta^{18}$O and water vapor exported from the tropics).

#### 3.3.3. Sea Surface Temperature Proxies ($\delta^{18}O_{calcite}$)

[47] The $\delta^{18}$O in the calcite shells ($\delta^{18}O_{calcite}$) of foraminifera can provide an estimate of ocean temperature if $\delta^{18}O_{seawater}$ is known. However, *LeGrande et al.* [2006] demonstrated that surface $\delta^{18}O_{calcite}$ anomalies across the northern North Atlantic ($\sim$40°–70°N) are not correlated with SST, in the years following the MWP, despite the temperature-dependent uptake of the heavier isotope during calcite precipitation.

[48] The cumulative effect of altered precipitation, decreased temperature, and reduced northward advection of salty, $\delta^{18}$O enriched waters cause all simulations to become fresher and more depleted in $\delta^{18}O_{seawater}$ in the central northern North Atlantic, but saltier and enriched in the GIN (Greenland, Iceland, Norwegian) seas and Arctic Ocean. Areas of enhanced salinity in these northern regions are generally associated with modest (tens of meters) deepening of the mixed layer depth.

[49] The reason that the $\delta^{18}O_{calcite}$-temperature proxy fails in much of the North Atlantic is that cooler temperatures cause enrichment in calcite ($\sim$0.2‰/°C) that balance the climate and MWP-related $\delta^{18}O_{seawater}$ depletion; the two cancel one another out. This modeled feature may explain the lack of clear, cold 8.2 ka event in $\delta^{18}O_{calcite}$ of many northern North Atlantic oceanic records, and it is supported by paired temperature (Mg/Ca) and $\delta^{18}O_{calcite}$ measurements [e.g., *Came et al.*, 2007; *Kleiven et al.*, 2008].

[50] North Atlantic SST anomalies vary from simulation to simulation (similar to Figure 3), but the majority exhibit GIN seas cooling, which leads to enriched $\delta^{18}O_{calcite}$. In this area of the ocean, $\delta^{18}O_{seawater}$ is enriched because of (1) increased sea ice formation or decreased sea ice melting and (2) less rainfall over the catchment basins for Arctic rivers (less delivery of a relatively enriched negative Arctic end-member); thus, the simulations predict that it should be much easier to detect a change in a GIN seas $\delta^{18}O_{calcite}$ records since both factors induce a $\delta^{18}O_{calcite}$ anomaly of the same sign. This finding matches well with proxy evidence from the east Norwegian seas, one of the few locations in the North Atlantic that has an abrupt 8.2 ka anomaly of +0.7‰ $\delta^{18}O_{calcite}$ [*Risebrobakken et al.*, 2003], and several of the simulations match this magnitude of signal. The phasing of the $\delta^{18}O_{calcite}$ signal (after the MWP release) is different in each simulation, and reflects the balance of prolonged positive, temperature-related anomalies, positive climate-related $\delta^{18}O_{seawater}$ anomalies, and short MWP-related negative anomalies. The ST simulations lack a positive $\delta^{18}O_{calcite}$ at the exact location of the *Risebrobakken et al.* [2003] core because the zonal front between the more depleted southern and more enriched northern surface $\delta^{18}O_{seawater}$ is slightly different in each simulation; though all simulations show a positive $\delta^{18}O_{calcite}$ anomaly slightly farther north. These experiments thus suggest that the best location for Atlantic 8.2 ka event records is in regions where the $\delta^{18}O_{seawater}$ and temperature signals cause anomalies in $\delta^{18}O_{calcite}$ of the same sign, such as enrichment in the GIN seas and northern northeastern Atlantic to Arctic Ocean.

[51] A more exact approach for comparing the modeled $\delta^{18}O_{calcite}$ to data during abrupt climate change would be to predict changes in individual species. *Schmidt and Mulitza* [2002] estimated the depth habitat of several species of planktonic foraminifera by using a core top data set coupled with oceanographic observations and made calculations for physical properties of the water column such as mixed layer depth. This analysis allows a calculation of the $\delta^{18}O_{calcite}$ in these specific planktonic foraminifer species given temperature, salinity, and $\delta^{18}O_{seawater}$ profiles. This solution was applied to all of the 8.2 ka simulations. However, it yielded enigmatic (inconsistent, unrealistic) results, probably owing to the extreme changes in physical properties of the ocean associated with the large surface density changes. Work to estimate changes in the oxygen isotopic composition of individual species of foraminifera during such a dramatic change in surface waters is ongoing.

#### 3.3.4. Paleosalinity Estimation

[52] Ocean salinity both plays an import role in determining ocean circulation (e.g., NADW formation) and provides an important indicator of the local freshwater balance, making it an important target for paleoceanographic studies. Since $\delta^{18}O_{seawater}$ is regionally linearly related to salinity, ocean proxy records of $\delta^{18}O_{calcite}$ are often corrected for temperature effects using an additional temperature proxy such as Mg/Ca. The result is used for reconstruction of past $\delta^{18}O_{seawater}$ variations, and paleosalinity is inferred given modern regional $\delta^{18}O_{seawater}$ to salinity relationships [*Schmidt et al.*, 2004; *Stott et al.*, 2004]. However, the relationship between $\delta^{18}O_{seawater}$ and salinity is controlled by the regional freshwater balance, and thus dependent on the freshwater end-members. Freshwater end-members are determined by the amount and isotopic composition of freshwater fluxes, including river runoff, precipitation, evaporation, sea ice, and atmospheric pathways (i.e., cross Panama isthmus transport) [*Schmidt*, 1999].

[53] During the 8.2 ka event, there is a potential for this relationship to change as (1) large alterations in sea ice formation (or decreased melting) occur, (2) MWP forcing (with its physical properties of $\delta^{18}O_{seawater}$: −30‰ and salinity: 0 psu) adds a significant amount of water with different physical properties, and (3) large-scale hydrologic cycle changes occur (i.e., the southward migration of the ITCZ, altered amount of tropical water export, changing location of precipitation bands, etc.).

[54] For each simulation, the temporal (decadal average) $\delta^{18}O_{seawater}$ to salinity relationships in the northern North Atlantic were determined. The temporal slope is different from the spatial slope, which is calculated from the range of $\delta^{18}O_{seawater}$ and salinity values within each region. The North Atlantic spatial slope in the WK case is 0.43‰/psu, near the ST case slope of 0.5‰/psu; these compare well to the observed 0.55‰/psu, but are slightly shallower [*LeGrande and Schmidt*, 2006].

[55] The freshwater end-member of the perturbed simulations could be simply thought of as a combination of the local freshwater end-member of the control (WK: −15, ST: −22) and the physical properties of the MWP (−30‰ $\delta^{18}$O and 0 psu); the perturbed freshwater end-members should fall within this range. However, the slope of the $\delta^{18}O_{seawater}$ to salinity curve becomes much steeper than a simple combination of the two, and the "intercept" of the curve (i.e., 0 psu as in the MWP) indicates a (super) depleted end-member, ∼−35 to −37‰. This more negative apparent end-member occurs because of diminished sea ice melting (increased formation); the WK case and the ST10 5 Sv × 2 year case also include advection of water that is fresher and depleted from the subtropics, pulling the curve steeper.

[56] This change not only hints at difficulties in reconstructing paleosalinity, but also in estimating freshwater end-members using such an approach (e.g., paired $\delta^{18}O_{calcite}$ and Mg/Ca measurements). In another study of climate response to altered orbital forcing (mid-Holocene to present), changes in this relationship over longer (millennial scale) time periods were shown to be possible [*Schmidt et al.*, 2007]. The fundamental point is that freshwater end-member changes due to climate change are not necessarily the same as those determined from spatial gradients.

#### 3.3.5. Surface Air Temperature and Precipitation Reconstructions

[57] Modern $\delta^{18}O_{precip}$ to SAT relationships are used for temperature reconstructions in middle- to high-latitude ice cores, speleothems, and lake records; whereas proxy precipitation amount (inversely related to $\delta^{18}O_{precip}$) is reconstructed from these records at low latitudes.

[58] The inverse precipitation relationship is simulated over Australia, South America, and Oman (Figure 8). However, this negative correlation between precipitation amount and $\delta^{18}O_{precip}$ does not exist in many locations. Regions with simulated cooling are also highly correlated with drying, similar to observations; i.e., ice core record correlation between lower temperature and lower accumulation [e.g., *Alley et al.*, 1997]. The combination of cooler temperatures (negative anomalies) and less precipitation (positive anomalies) not only works to dampen $\delta^{18}O_{precip}$ signals, but also creates an "artifact" of a positive relationship between $\delta^{18}O_{precip}$ and precipitation amount. Precipitation amount over the Greenland and Antarctic ice sheets is highly positively correlated to $\delta^{18}O_{precip}$, an artifact of cooling.

[59] The modern relationship between SAT and $\delta^{18}O_{precip}$ across Greenland, or the spatial slope, is roughly twice the inferred temporal relationship between the two at the Summit location alone, or temporal slope of 0.3‰/°C [*Cuffey et al.*, 1995]. The modeled temporal slope of $\delta^{18}O_{precip}$ versus SAT at Summit, around 0.25–0.35‰/°C, is near this inferred temporal slope. Vostok and the rest of Antarctica have temporal slopes around 0.2–0.3‰/°C; the spatial slope across Antarctica is ∼0.79‰/°C, similar to the observed spatial slope (similar to temporal slope in Antarctica) of 0.7‰/°C [*Jouzel et al.*, 2003].

#### 3.3.6. Proxy to Model Comparisons

[60] Decadal temperature, precipitation, and $\delta^{18}O_{precip}$ anomalies at locations with proxies having a clear 8.2 ka event (Figure 9) are in reasonable agreement with proxy records [*Alley and Ágústsdóttir*, 2005]. Locations in the immediate vicinity of the North Atlantic basin have the most consistent cooling response (across all simulations) to the MWP forcing, but are highly variable in their magnitude. There is good agreement between locations with known 8.2 ka event decadal $\delta^{18}O_{precip}$ anomalies; however, it is important to note that the $\delta^{18}O_{precip}$ anomalies are more complicated than either temperature or precipitation anomalies alone (Figure 9). In general, the simulations with the smallest MWP forcing have the worst match to observations.

[61] The annual range of $\delta^{18}O_{precip}$ anomalies at Summit, Greenland (−3 to −1.2‰) [*LeGrande et al.*, 2006] bracket the observed −2‰ [*Alley et al.*, 1997] though decadal anomalies are ∼1/2 the magnitude. Ammersee (observed −1‰ [*von Grafenstein et al.*, 1998]) $\delta^{18}O_{precip}$ decreases by up to −0.6‰ but is enriched in some simulations where the front between negative European and positive Mediterranean $\delta^{18}O_{precip}$ is shifted somewhat to the north. The British Isles show large depletion in $\delta^{18}O_{precip}$, consistent with an ∼−1‰ anomaly identified in lake records [*Marshall et al.*, 2007]. Large negative signals in $\delta^{18}O_{precip}$ occur in the immediate vicinity of the North Atlantic, and the simulations suggest that mid to northern Europe will be the best place to look for records of the 8.2 ka event.

[62] Proxy records that capture ITCZ changes in China are likely to show a positive $\delta^{18}O_{calcite}$ anomaly given that most simulations exhibit positive (though small) anomalies; speleothem $\delta^{18}O_{calcite}$ records from Dongge, China [*Wang et al.*, 2005], and Oman [*Fleitmann et al.*, 2003] have been interpreted as a weakening of the monsoon; simulated $\delta^{18}O_{precip}$ anomalies are generally positive over Asia, though small or of opposite sign along the coast. Speleothems in other tropical locations such as Brazil would be expected to begin precipitating or become more negative in $\delta^{18}O_{calcite}$ because of a southward migration of the ITCZ.

## 4. Discussion and Conclusions

[63] The model simulations do not exactly reproduce the 8.2 ka event. However, they indicate that the robust response to freshwater forcing across all simulations, a reduction in NADW, is consistent with the proxy signal; furthermore, other paired experiments [*LeGrande et al.*, 2006] indicate an ∼50% reduction in NADW formation is most consistent with multiple types of proxy records, constraining the past climate response to large freshwater forcing. The better match of the WK case to proxy records suggests a lack of deep convection in the Labrador Sea is an important factor to modulating the climate response at 8.2 ka, though the reasons that model lacks convection here are not the same as in the early Holocene.

[64] A MWP pulse of the duration and magnitude suggested by previous geologic and paleohydraulic studies [*Barber et al.*, 1999; *Clarke et al.*, 2004] initiates a reduction of NADW in the GISS model; this modeled climate response consistent with multiple proxy records [*Alley et al.*, 1997; *Leuenberger et al.*, 1999; *von Grafenstein et al.*, 1998; *etc.*]. This study, therefore, supports the idea that an alteration in ocean circulation and resulting climate response were very

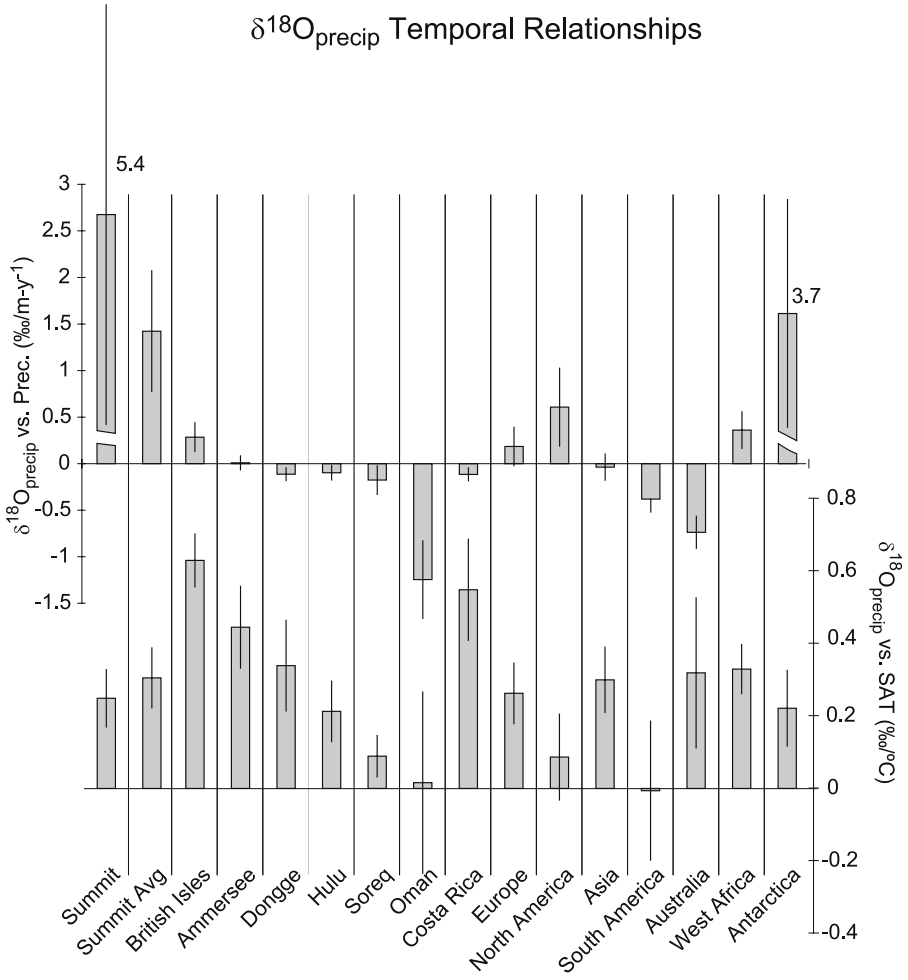


**Figure 8.** The anomalies in $\delta^{18}O_{precip}$ divided by (top) precipitation (m/a) (bars) and (bottom) SAT (°C) (bars) at locations around the world for the ensemble set of simulations (see Table 1). The $\sigma_{slope}$ at these locations is the error line imposed on each bar. Goodness of fit is generally good where the slope is higher. Summit average includes Summit and the adjacent south and east boxes.

likely associated with the 8.2 ka event observed in North Atlantic region proxy records.

[65] The differences within each individual realization, notably the failure of any single one simulation to provide the best fit to all proxy records, demonstrates the value of an ensemble of simulations. Furthermore, the ensemble allows the separation of the climate response to a reduction in NADW from internal model variability. Importantly, the climate response was nonlinear (or perhaps stochastic), in that the largest volume and fastest rates of input were not the sole predictors of the magnitude and length of the simulated climate responses. In addition, anomalies in different fields (SAT, precipitation, etc.) displayed varying magnitudes and extent such that the simulation with largest anomaly in one field did not necessarily have the greatest anomaly in another. Also, the decadal variability exhibited by the model hints at the limits of predictability given decadal noise.

[66] The base state of the climate (illustrated by the ST case and WK case simulations) is very important in controlling the impact of freshwater forcing. Though climate changes related to NADW formation changes have a robust pattern, the magnitude of the change, and feedbacks that are initiated by alterations in ocean circulation are dependent on the initial state of the climate. The NADW of the WK case may more closely emulate the early Holocene than the ST case since it lacks deep convection in the Labrador Sea Water; however, climate anomalies associated with purely the slowdown in overturning circulation are more clearly exhibited in the ST case. The range of both cases in feedbacks and in the conditions consistent with the production of Labrador Sea Water make the analysis of the two together more instructive than either alone. Importantly, the greater transport of salt and heat from the Indian Ocean into the Atlantic as well as the weaker vertical ocean stratification of the ST case make it less susceptible to prolonged (100+ years) climate change.

[67] Previous studies of the 8.2 ka event have suggested that multiple cooling episodes, or spikes, in proxy records [e.g., *Alley et al.*, 1997; *Ellison et al.*, 2006] indicate glacial lakes Agassiz and Ojibway drained in multiple stages. Although there is some geologic evidence for a two-stage

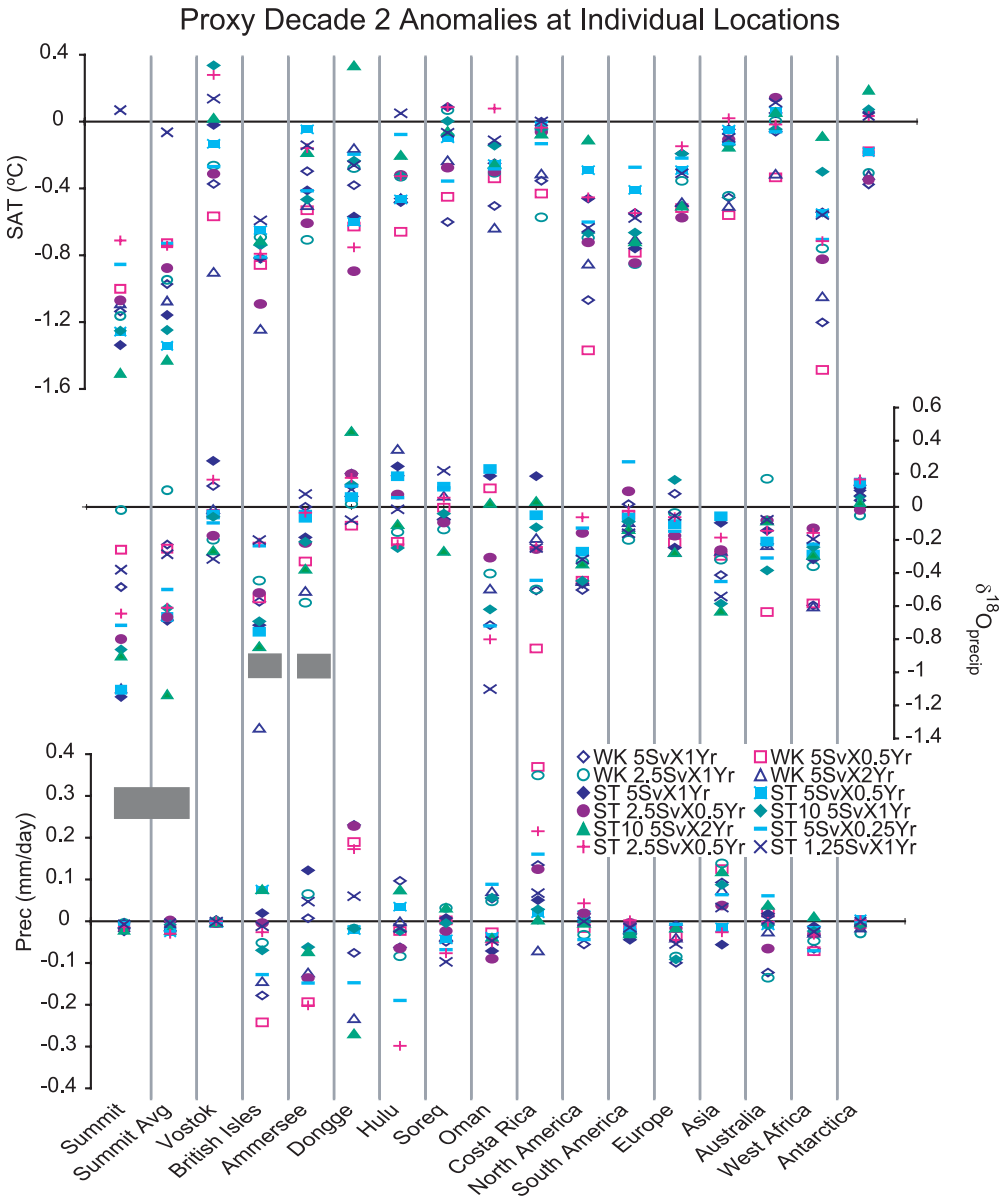


**Figure 9.** Decade 2 (top) surface air temperature (°C), (middle) $\delta^{18}O_{precip}$ (‰), and (bottom) precipitation (mm/d) anomalies from each of the 12 simulations. Water isotopes in precipitation are generally thought to record to reflect temperature and precipitation. Summit average includes Summit and the adjacent south and east boxes. Large gray boxes indicate $\delta^{18}O_{precip}$ values from select sites [*Alley et al.*, 1997; *Marshall et al.*, 2007; *von Grafenstein et al.*, 1998].

drainage [*Teller et al.*, 2002], the phasing of simulated meltwater rain out (Figure 6) and multiple reductions in overturning circulation (Figure 1) indicate that two stages of drainage are not necessarily required to produce multiple cooling events in proxy records. About 1/3 of the simulations (depending on the threshold for "signal" used) clearly display multiple cooling episodes, in response to the single MWP forcing in each. Thus, multiple drainage events cannot be supported or ruled out given these results, though they are apparently not required to produce multiple stages of climate response.

[68] The maximum change in NADW formation is not concurrent with the maximum change of surface density; NADW formation is associated with the density gradients in the ocean. Far-field mechanisms for restoring NADW production such as the advection of salt from the tropics or South Atlantic do not appear to reinitiate NADW in these simulations. Rather, NADW formation is restored through mixing the freshwater signal away (dilution) and through regional atmospheric feedbacks that cause the surface freshwater balance (P − E + R) of the ocean to become more negative.

[69] Water isotope tracers in the model allow the simulations to be compared directly to water isotope proxies of this last major abrupt climate change. The largest atmospheric perturbations in the oxygen isotopic composition of precipitation occur around the North Atlantic basin, similar

to observed [*Schmidt and Jansen*, 2006]. The modeled signal over land is strongest (1) in Europe and Greenland because of strong regional cooling and (2) in the tropical Atlantic because of the southward migration of the ITCZ. The latter results in enriched northern and depleted southern bands, consistent with multiple proxy records of the 8.2 ka event [*Alley and Ágústsdóttir*, 2005; *Arz et al.*, 2001; *Haug et al.*, 2001]. Simulated signals are generally small or very short-lived (<40 years).

[70] The relationship of proxies to climate is very important to infer paleoclimate from proxy records. These simulations provide an opportunity to quantify it during a transient, abrupt climate change event. The regression between the oxygen isotopic composition of precipitation and temperature is strongest in the midlatitudes. Interestingly, the rain out of isotopically depleted meltwaters, as well as the sensitivity to precipitation amount, causes the correlation to temperature at many sites, particularly Summit, Greenland, to be poor, especially in the first decade after the MWP. In the tropics, the oxygen isotopic composition of precipitation does faithfully record the southward migration of the ITCZ. However, the relationship between precipitation amount to $\delta^{18}O_{precip}$ is not constant across the tropics, pointing to the importance of larger-scale climate dynamics, such as the tropical hydrologic cycle, in determining $\delta^{18}O_{precip}$ [*Schmidt et al.*, 2007]. Given this issue, interpretations of $\delta^{18}O_{precip}$ changes as local precipitation over long time scales may be misleading.

## 5. Future Improvements

[71] In all modeling of these kinds of events, certain simplifications must be made. For instance, the drainage of glacial Lakes Agassiz and Ojibway likely behaved in a different manner than is simulated in the model. The ice dam collapsed from the bottom up, beginning with flow underneath the ice sheet, similar to modern jökulhlaups [*Clarke et al.*, 2004]. This type of flow would have been laden with sediment, initially denser than the surrounding seawater, and thus potentially injected at a deeper level. The residence time of this type of sediment in the water column is relatively short [*Kerwin*, 1996]; as soon as the sediments settled out of the meltwater, there would have been a freshwater plume of the meltwater back to the surface since the overlying seawater is much denser than the sediment free fresh water.

[72] The drainage of these two glacial lakes into the open ocean most probably occurred as a boundary current that tracked southward, along the Labrador coast [*Keigwin et al.*, 2005]. The coarse resolution of the GISS ocean model prevents it from resolving this type of current. Additional simulations could be performed where the location of the MWP (and perhaps it physical properties) were altered to account for this process. Alternatively, simulations could be performed on a much higher resolution, most likely regional, ocean model to establish the behavior of the meltwater and boundary current, and then these results could be used to force a coarser resolution coupled GCM.

[73] It is possible that additional mixing could have occurred during this process, and have altered the physical properties of the meltwater. Additional simulations could be performed where fresh water is injected at deeper levels in the Hudson Bay; however, this change would be unlikely to affect the results as has been discussed above, the initial large density contrast between the MWP and the seawater does not coincide with the maximum decrease in NADW formation. The large temperature and salinity anomalies quickly dissipate. It is the later smaller magnitude surface density changes that are associated with the largest decreases of NADW. However, since the boundary currents could delay the injection of the meltwater into the open ocean, one possible outcome would be an alteration in the phasing, or a lag, of response time in the climate after the initial MWP, on the order of a few months.

[74] However, it is unlikely that these additional simulations in the current version of the model would have yielded results that are different than those presented here. Two other freshwater forcing scenarios (though with different volumes and rates of input) have been performed on this configuration of the model. In the first, fresh water is added to the Arctic Ocean, and in the second, fresh water is spread over the open northern North Atlantic, as in the hosing PMIP (Paleoclimate Model Intercomparison Project) experiments [*Stouffer et al.*, 2006]. Essentially, the model responds at a decadal mean time scale whenever fresh water is advected over deepwater formation sites. Changing the location of the initial forcing only serves to alter the timing between the initial pulse and subsequent climate response. The way to determine the significance of boundary current and sediment loading in models is to use significantly higher resolution which is not currently available, but may become so in the future.

[75] Not included in this study were several boundary conditions relevant to the period 8000 years ago. Future simulations will undoubtedly include these three changes (orbital, orography, and greenhouse gases) as boundary conditions. Orbital forcing 8000 years ago was different from the preindustrial with the Earth's axis tilting more steeply than at present and boreal summer coinciding more closely with the perihelion. These changes would have resulted in around 9.4% more insolation during June at 65°N [*Berger and Loutre*, 1991], and this change may have affected the seasonality of the climate response. Since deepwater formation dampens wintertime cooling, and seasonality was greater at 8-ka, responses to freshwater perturbations in winter may have been stronger. It is possible that the lack of an abrupt orographic change, the collapse of the Hudson Bay ice dome, caused some of the model simulations to underestimate the magnitude of anomaly indicated by proxy records. Surface albedo and runoff from the ice sheet itself, may have primed the ocean to respond differently.

[76] Greenhouse gases were slightly lower in the early Holocene compared to the recent preindustrial. $CO_2$ was about 25 ppm lower, and though methane concentrations were similar initially, the 8.2 ka event itself includes a 75 ppbv decrease in methane [*Kobashi et al.*, 2007]. A future coupled model study might also include interactive methane since it might have played a role in enhancing the cooling as well as altering the pattern, length, or magnitude

of the climate. Reduced methane concentration at 8.2 ka is consistent with our previous simulations [*LeGrande et al.*, 2006], but the methane feedback was not included in the response (the magnitude of this feedback is small, a global radiative forcing of $\sim$0.04 W/m$^2$).

[77] The 8.2 ka cooling event was coincident with the largest freshwater pulse of the last deglaciation [*Barber et al.*, 1999; *Dyke*, 2004]. Its occurrence with near present-day boundary conditions and short duration present an excellent opportumnity for a case study for evaluating model skill [*Schmidt and LeGrande*, 2005]. We encourage other willing groups to do similar experiments in order to test the robustness of our conclusions.

[78] **Acknowledgments.** The support for A.N.L. and G.A.S. was provided from NSF grant ATM-05-01241. Support for A.N.L. was also provided from a NDSEG graduate student fellowship. We thank three anonymous reviewers who helped to significantly improve the clarity of the manuscript.

## References

Alley, R. B., and A. M. Ágústsdóttir (2005), The 8k event: Cause and consequences of a major Holocene abrupt climate change, *Quat. Sci. Rev.*, *24*(10–11), 1123–1149, doi:10.1016/j.quascirev.2004.12.004.

Alley, R. B., P. A. Mayewski, T. Sowers, M. Stuiver, K. C. Taylor, and P. U. Clark (1997), Holocene climatic instability: A prominent, widespread event 8200 yr ago, *Geology*, *25*(6), 483–486, doi:10.1130/0091-7613(1997)025<0483:HCIAPW>2.3.CO;2.

Arz, H. W., S. Gerhardt, J. Patzold, and U. Röhl (2001), Millennial-scale changes of surface- and deep-water flow in the western tropical Atlantic linked to Northern Hemisphere high-latitude climate during the Holocene, *Geology*, *29*(3), 239–242, doi:10.1130/0091-7613(2001)029<0239:MSCOSA>2.0.CO;2.

Barber, D. C., et al. (1999), Forcing of the cold event of 8,200 years ago by catastrophic drainage of Laurentide lakes, *Nature*, *400*(6742), 344–348, doi:10.1038/22504.

Bauer, E., A. Ganopolski, and M. Montoya (2004), Simulation of the cold climate event 8200 years ago by meltwater outburst from Lake Agassiz, *Paleoceanography*, *19*, PA3014, doi:10.1029/2004PA001030.

Berger, A., and M. F. Loutre (1991), Insolation values for the climate of the last 10 million years, *Quat. Sci. Rev.*, *10*(4), 297–317, doi:10.1016/0277-3791(91)90033-Q.

Broecker, W. S. (1998), Paleocean circulation during the last deglaciation: A bipolar seesaw?, *Paleoceanography*, *13*(2), 119–121, doi:10.1029/97PA03707.

Broecker, W. S., and G. H. Denton (1990), The role of ocean-atmosphere reorganizations in glacial cycles, *Quat. Sci. Rev.*, *9*(4), 305–341, doi:10.1016/0277-3791(90)90026-7.

Broecker, W. S., D. M. Peteet, and D. Rind (1985), Does the ocean-atmosphere system have more than one stable mode of operation, *Nature*, *315*(6014), 21–26, doi:10.1038/315021a0.

Came, R. E., D. W. Oppo, and J. F. McManus (2007), Amplitude and timing of temperature and salinity variability in the subpolar North Atlantic over the past 10 k.y, *Geology*, *35*(4), 315–318, doi:10.1130/G23455A.1.

Clarke, G. K. C., D. W. Leverington, J. T. Teller, and A. S. Dyke (2004), Paleohydraulics of the last outburst flood from glacial Lake Agassiz and the 8200 B. P. cold event, *Quat. Sci. Rev.*, *23*(3–4), 389–407, doi:10.1016/j.quascirev.2003.06.004.

Conkright, M. E., R. A. Locarnini, H. E. Garcia, T. D. O'Brien, T. P. Boyer. C. Stephens and J. I. Antonov (2002), World Ocean Atlas 2001: Objective Analyses, Data Statistics, and Figures CD-ROM Documentation, *Internal Rep. 17*, pp. 1–21, Natl. Oceanogr. Data Cent., Silver Spring, Md.

Craig, H., and L. I. Gordon (1965), *Deuterium and Oxygen 18 Variations in the Ocean and the Marine Atmosphere*, Cons. Naz. Delle Nucl., Pisa, Italy.

Cuffey, K. M., G. D. Clow, R. B. Alley, M. Stuiver, E. D. Waddington, and R. W. Saltus (1995), Large Arctic temperature-change at the Wisconsin-Holocene glacial transition, *Science*, *270*(5235), 455–458, doi:10.1126/science.270.5235.455.

Dyke, A. S. (2004), An outline of North American deglaciation with emphasis on central and northern Canada, in *Quaternary Glaciations—Extent and Chronology, Part II: North America*, edited by J. Ehlers and P. L. Gibbard, pp. 371–406, Elsevier, Amsterdam.

Ellison, C. R. W., M. R. Chapman, and I. R. Hall (2006), Surface and deep ocean interactions during the cold climate event 8200 years ago, *Science*, *312*(5782), 1929–1932, doi:10.1126/science.1127213.

Fleitmann, D., S. J. Burns, M. Mudelsee, U. Neff, J. Kramers, A. Mangini, and A. Matter (2003), Holocene forcing of the Indian monsoon recorded in a stalagmite from southern Oman, *Science*, *300*(5626), 1737–1739, doi:10.1126/science.1083130.

Haug, G. H., K. A. Hughen, D. M. Sigman, L. C. Peterson, and U. Röhl (2001), Southward migration of the intertropical convergence zone through the Holocene, *Science*, *293*(5533), 1304–1308, doi:10.1126/science.1059725.

Hillaire-Marcel, C., and A. de Vernal (1995), Mais que s'est $\sim$ il donc passé vers 8,000 ans BP?, paper presented at Annual Meeting, Assoc. Québec Etude Quat., Montreal, Que., Canada.

Hillaire-Marcel, C., A. de Vernal, G. Bilodeau, and A. J. Weaver (2001), Absence of deep-water formation in the Labrador Sea during the last interglacial period, *Nature*, *410*(6832), 1073–1077, doi:10.1038/35074059.

Jouzel, J., F. Vimeux, N. Caillon, G. Delaygue, G. Hoffmann, V. Masson-Delmotte, and F. Parrenin (2003), Magnitude of isotope/temperature scaling for interpretation of central Antarctic ice cores, *J. Geophys. Res.*, *108*(D12), 4361, doi:10.1029/2002JD002677.

Keigwin, L. D., J. P. Sachs, Y. Rosenthal, and E. A. Boyle (2005), The 8200 year BP event in the slope water system, western subpolar North Atlantic, *Paleoceanography*, *20*, PA2003, doi:10.1029/2004PA001074.

Kerwin, M. W. (1996), A regional stratigraphic isochron (ca. 8000 $^{14}$C yr B.P.) from final deglaciation of Hudson Strait, *Quat. Res.*, *46*(2), 89–98, doi:10.1006/qres.1996.0049.

Kleiven, H. F., C. Kissel, C. Laj, U. S. Ninnemann, T. O. Richter, and E. Cortijo (2008), Reduced North Atlantic Deep Water coeval with the glacial Lake Agassiz fresh water outburst, *Science*, *319*(5859), 60–64, doi:10.1126/science.1148924.

Kobashi, T., J. P. Severinghaus, E. J. Brook, J.-M. Barnola, and A. M. Grachev (2007), Precise timing and characterization of abrupt climate change 8200 years ago from air trapped in polar ice, *Quat. Sci. Rev.*, *26*(9–10), 1212–1222, doi:10.1016/j.quascirev.2007.01.009.

LeGrande, A. N., and G. A. Schmidt (2006), Global gridded dataset of the oxygen isotopic composition in seawater, *Geophys. Res. Lett.*, *33*, L12604, doi:10.1029/2006GL026011.

LeGrande, A. N., G. A. Schmidt, D. T. Shindell, C. V. Field, R. L. Miller, D. M. Koch, G. Faluvegi, and G. Hoffmann (2006), Consistent simulations of multiple proxy responses to an abrupt climate change event, *Proc. Natl. Acad. Sci. U.S.A.*, *103*(4), 837–842, doi:10.1073/pnas.0510095103.

Leuenberger, M. C., C. Lang, and J. Schwander (1999), Delta $^{15}$N measurements as a calibration tool for the paleothermometer and gas-ice age differences: A case study for the 8200 BP event on GRIP ice, *J. Geophys. Res.*, *104*(D18), 22,163–22,170, doi:10.1029/1999JD900436.

Liu, J. P., G. A. Schmidt, D. G. Martinson, D. Rind, G. Russell, and X. J. Yuan (2003), Sensitivity of sea ice to physical parameterizations in the GISS global climate model, *J. Geophys. Res.*, *108*(C2), 3053, doi:10.1029/2001JC001167.

Marshall, J. D., et al. (2007), Terrestrial impact of abrupt changes in the North Atlantic thermohaline circulation: Early Holocene, UK, *Geology*, *35*(7), 639–642, doi:10.1130/G23498A.1.

Masson, V., et al. (2000), Holocene climate variability in Antarctica based on 11 ice-core isotopic records, *Quat. Res.*, *54*(3), 348–358, doi:10.1006/qres.2000.2172.

Morrill, C., and R. M. Jacobsen (2005), How widespread were climate anomalies 8200 years ago?, *Geophys. Res. Lett.*, *32*, L19701, doi:10.1029/2005GL023536.

Open University Course Team (2001), *Ocean Circulation*, 2nd ed., edited by G. Bearman, Elsevier, New York.

Pfirman, S., W. Haxby, H. Eicken, M. Jeffries, and D. Bauch (2004), Drifting Arctic sea ice

archives changes in ocean surface conditions, *Geophys. Res. Lett.*, *31*, L19401, doi:10.1029/2004GL020666.

Randall, D. A. W. R. A., et al. (2007), Climate models and their evaluation, in *Climate Change 2007: The Physical Science Basis: Contribution of Working Group I to the Fourth Assessment Report of the Intergovernmental Panel on Climate Change*, edited by S. Solomon et al., pp. 589–662, Cambridge Univ. Press, Cambridge, U. K.

Renssen, H., H. Goosse, T. Fichefet, and J. M. Campin (2001), The 8.2 kyr BP event simulated by a global atmosphere–sea-ice–ocean model, *Geophys. Res. Lett.*, *28*(8), 1567–1570, doi:10.1029/2000GL012602.

Renssen, H., H. Goosse, and T. Fichefet (2002), Modeling the effect of freshwater pulses on the early Holocene climate: The influence of high-frequency climate variability, *Paleoceanography*, *17*(2), 1020, doi:10.1029/2001PA000649.

Rind, D., P. deMenocal, G. Russell, S. Sheth, D. Collins, G. Schmidt, and J. Teller (2001), Effects of glacial meltwater in the GISS coupled atmosphere ocean model: 1. North Atlantic Deep Water response, *J. Geophys. Res.*, *106*(D21), 27,335–27,353, doi:10.1029/2000JD000070.

Risebrobakken, B., E. Jansen, C. Andersson, E. Mjelde, and K. Hevroy (2003), A high-resolution study of Holocene paleoclimatic and paleoceanographic changes in the Nordic Seas, *Paleoceanography*, *18*(1), 1017, doi:10.1029/2002PA000764.

Rohling, E. J., and H. Pälike (2005), Centennial-scale climate cooling with a sudden cold event around 8,200 years ago, *Nature*, *434*(7036), 975–979, doi:10.1038/nature03421.

Russell, G. L., J. R. Miller, and D. Rind (1995), A coupled atmosphere-ocean model for transient climate change studies, *Atmos. Ocean*, *33*(4), 683–730.

Russell, G. L., J. R. Miller, D. Rind, R. A. Ruedy, G. A. Schmidt, and S. Sheth (2000), Comparison of model and observed regional temperature changes during the past 40 years, *J. Geophys. Res.*, *105*(D11), 14,891–14,898, doi:10.1029/2000JD900156.

Schmidt, G. A. (1999), Error analysis of paleosalinity calculations, *Paleoceanography*, *14*(3), 422–429, doi:10.1029/1999PA900008.

Schmidt, G. A., and E. Jansen (2006), The 8.2kyr event, *PAGES News*, *14*, 28–29.

Schmidt, G. A., and A. N. LeGrande (2005), The Goldilocks abrupt climate change event, *Quat. Sci. Rev.*, *24*(10–11), 1109–1110, doi:10.1016/j.quascirev.2005.01.015.

Schmidt, G. A., and S. Mulitza (2002), Global calibration of ecological models for planktic foraminifera from coretop carbonate oxygen-18, *Mar. Micropaleontol.*, *44*(3–4), 125–140, doi:10.1016/S0377-8398(01)00041-X.

Schmidt, M. W., H. J. Spero, and D. W. Lea (2004), Links between salinity variation in the Caribbean and North Atlantic thermohaline circulation, *Nature*, *428*(6979), 160–163, doi:10.1038/nature02346.

Schmidt, G. A., G. Hoffmann, D. T. Shindell, and Y. Hu (2005), Modeling atmospheric stable water isotopes and the potential for constraining cloud processes and stratosphere-troposphere water exchange, *J. Geophys. Res.*, *110*, D21314, doi:10.1029/2005JD005790.

Schmidt, G. A., et al. (2006), Present day atmospheric simulations using GISS ModelE: Comparison to in situ, satellite, and reanalysis data, *J. Clim.*, *19*(2), 153–192, doi:10.1175/JCLI3612.1.

Schmidt, G. A., A. N. LeGrande, and G. Hoffmann (2007), Water isotope expressions of intrinsic and forced variability in a coupled ocean-atmosphere model, *J. Geophys. Res.*, *112*, D10103, doi:10.1029/2006JD007781.

Stott, L., K. Cannariato, R. Thunell, G. H. Haug, A. Koutavas, and S. Lund (2004), Decline of surface temperature and salinity in the western tropical Pacific Ocean in the Holocene epoch, *Nature*, *431*(7004), 56–59, doi:10.1038/nature02903.

Stouffer, R., et al. (2006), Investigating the causes of the response of the thermohaline circulation to past and future climate changes, *J. Clim.*, *19*(8), 1365–1387, doi:10.1175/JCLI3689.1.

Teller, J. T., D. W. Leverington, and J. D. Mann (2002), Freshwater outbursts to the oceans from glacial Lake Agassiz and their role in climate change during the last deglaciation, *Quat. Sci. Rev.*, *21*(8–9), 879–887, doi:10.1016/S0277-3791(01)00145-7.

Thomas, E. R., E. W. Wolff, R. Mulvaney, J. P. Steffensen, S. J. Johnsen, C. Arrowsmith, J. W. C. White, B. Vaughn, and T. Popp (2007), The 8.2 ka event from Greenland ice cores, *Quat. Sci. Rev.*, *26*(1–2), 70–81, doi:10.1016/j.quascirev.2006.07.017.

von Grafenstein, U., H. Erlenkeuser, J. Muller, J. Jouzel, and S. Johnsen (1998), The cold event 8200 years ago documented in oxygen isotope records of precipitation in Europe and Greenland, *Clim. Dyn.*, *14*(2), 73–81, doi:10.1007/s003820050210.

Wang, Y. J., H. Cheng, R. L. Edwards, Y. Q. He, X. G. Kong, Z. S. An, J. Y. Wu, M. J. Kelly, C. A. Dykoski, and X. D. Li (2005), The Holocene Asian monsoon: Links to solar changes and North Atlantic climate, *Science*, *308*(5723), 854–857, doi:10.1126/science.1106296.

Wiersma, A. P., and H. Renssen (2006), Model-data comparison for the 8.2 ka BP event: Confirmation of a forcing mechanism by catastrophic drainage of Laurentide lakes, *Quat. Sci. Rev.*, *25*(1–2), 63–88, doi:10.1016/j.quascirev.2005.07.009.

Wiersma, A. P., H. Renssen, H. Goosse, and T. Fichefet (2006), Evaluation of different freshwater forcing scenarios for the 8.2 ka BP event in a coupled climate model, *Clim. Dyn.*, *27*(7–8), 831–849, doi:10.1007/s00382-006-0166-0.

Zhang, R., and T. L. Delworth (2005), Simulated tropical response to a substantial weakening of the Atlantic thermohaline circulation, *J. Clim.*, *18*(12), 1853–1860, doi:10.1175/JCLI3460.1.

A. N. LeGrande and G. A. Schmidt, Center for Climate Systems Research, NASA Goddard Institute for Space Studies, 2880 Broadway, New York, NY 10025, USA. (legrande@giss.nasa.gov)